



NEUTRONICS DESIGN STUDY ON A MINOR ACTINIDE  
BURNER FOR TRANSMUTING SPENT FUEL

August 1998

30 - 48

KOREA ATOMIC ENERGY RESEARCH INSTITUTE

R

제 출 문

한국원자력연구소장 귀하

본 보고서를 1998 년도 “DUPIC 핵연료 양립성평가 기술개발” 과제의 기술보고서로 제출  
합니다.

1998년 8월 일

과 제 명 : DUPIC 핵연료 양립성평가

주 저 자 : 최 항 복

공 저 자 :

감수위원 : 김 공 구

KAERI/TR-1111/98

**Neutronics Design Study on a Minor Actinide Burner  
for Transmuting Spent Fuel**

by

Hangbok Choi

August 1998

Korea Atomic Energy Research Institute  
P.O. Box 105, Yuseong  
Taejon, Korea, 305-600

**NEUTRONICS DESIGN STUDY ON A MINOR ACTINIDE BURNER  
FOR TRANSMUTING SPENT FUEL**

Hangbok Choi

Korea Atomic Energy Research Institute  
P.O. Box 105, Yuseong  
Taejon, 305-600, Korea

**ABSTRACT**

A liquid metal reactor was designed for the primary purpose of burning the minor actinide waste from commercial light water reactors. The design was constrained to maintain acceptable safety performance as measured by the burnup reactivity swing, the doppler coefficient, and the sodium void worth. Sensitivity studies were performed for homogeneous and decoupled core designs, and a minor actinide burner design was determined to maximize actinide consumption and satisfy safety constraints. One of the principal innovations was the use of two core regions, with a fissile plutonium outer core and an inner core consisting only of minor actinides. The physics studies performed here indicate that a 1200 MWth core is able to transmute the annual minor actinide inventory of about 16 LWRs and still exhibit reasonable safety characteristics.

## TABLE OF CONTENTS

SECTION	PAGE
ABSTRACT .....	1
I. INTRODUCTION .....	8
II. DESIGN MORPHOLOGY .....	11
II.1 Design Criteria .....	11
II.2 Cross-Section Data .....	12
II.3 Fuel Cycle Model .....	12
II.3.1 In-Core Fuel Cycle .....	13
II.3.2 Ex-Core Fuel Cycle .....	14
II.4 Safety Performance Parameters .....	14
II.4.1 Burnup Reactivity Swing .....	14
II.4.2 Sodium Void Worth .....	15
II.4.3 Doppler Constant ( $K_D$ ) .....	16
III. HOMOGENEOUS MINOR ACTINIDE BURNER DESIGN .....	17
III.1 Base Minor Actinide Burner Model .....	18
III.2 Effect of Fuel Cycle Length .....	19
III.3 Effect of Sodium Fraction and Core Size .....	20
III.3.1 Sodium Fraction .....	20
III.3.2 Core Size for High Sodium Fraction Assembly .....	20
III.4 Effect of Moderating Material .....	21
III.5 Effect of Reactor Power .....	21
III.6 Effect of Core Geometry .....	22
III.6.1 Reduced Core Height .....	22
III.6.2 Annular Core Model .....	23
III.7 Summary .....	24

IV. DECOUPLED MINOR ACTINIDE BURNER DESIGN ..... 26

    IV.1 Base Decoupled Core ..... 26

    IV.2 Effect of Moderating Material ..... 27

    IV.3 Effect of Outer Core Size ..... 28

V. FINAL CORE MODEL ..... 29

    V.1 Fuel Cycle ..... 29

    V.2 Safety Performance Parameters ..... 30

    V.3 Estimation of Fuel Temperature ..... 31

    V.4 Summary ..... 33

VI. SUMMARY, CONCLUSIONS, AND RECOMMENDATIONS ..... 35

REFERENCES ..... 37

TABLES	PAGE
Table I. Nominal Design Parameters of MAB .....	41
Table II. Isotopic Composition of Discharged Fuel from 1000 MWe LWR after 3 Years Cooling .....	42
Table III. Characteristics of Homogeneous Base Core .....	43
Table IV. Characteristics of Homogeneous Base Core .....	44
Table V. Effect of Cycle Length .....	45
Table VI. Effect of Sodium Fraction .....	46
Table VII. Effect of Core Size for High Sodium Fraction (0.727) Core .....	47
Table VIII. Effect of Moderating Pins .....	48
Table IX. Effect of Reactor Power and Size .....	49
Table X. Effect of Core Height .....	50
Table XI. Effect of Annular Geometry .....	51
Table XII. Characteristics of Decoupled Base Core .....	52
Table XIII. Fuel Composition of Decoupled Base Core .....	53
Table XIV. Effect of Moderating Pins in Outer Core .....	54
Table XV. Effect of Outer Core Size .....	55
Table XVI. General Specifications of Final MAB Model .....	56
Table XVII. Fuel Assembly Data of Final MAB Model .....	57
Table XVIII. Fuel Composition of Final MAB Model .....	58
Table XIX. Equilibrium Cycle Performance Parameter of Final MAB Model .....	59
Table XX. Safety Performance Parameters of Final MAB Model .....	60
Table XXI. Thermal Property Data .....	61
Table XXII. Effect of Outer Core Pin Size in Final MAB Model .....	62

FIGURES	PAGE
Fig.1 Mass Flow of MAB Fuel Cycle .....	63
Fig.2 Horizontal View of Homogeneous Base Core .....	64
Fig.3 Vertical View of Homogeneous Base Core .....	65
Fig.4 Homogeneous Core Model with a Sodium Fraction of 0.469 .....	66
Fig.5 Homogeneous Core Model with a Sodium Fraction of 0.567 .....	67
Fig.6 Homogeneous Core Model with a Sodium Fraction of 0.727 .....	68
Fig.7 Spectrum Softening due to Sodium Fraction .....	69
Fig.8 Spectrum Softening due to Moderating Pins .....	70
Fig.9 Annular Core Model .....	71
Fig.10 Decoupled Base Core Model .....	72
Fig.11 Horizontal View of Final MAB Model .....	73
Fig.12 Vertical View of Final MAB Model .....	74
Fig.13 Spectrum Hardening in Inner Core .....	75
Fig.14 Spectrum Hardening in Outer Core .....	76



## I. INTRODUCTION

For the last 40 years, the utilization of nuclear power has resulted in an accumulation of solidified high-level wastes. The hazard from the high level waste can be classified into two sources such as fission products and actinides. The short-term hazard is dominated by the  $^{90}\text{Sr}$  and  $^{137}\text{Cs}$  fission products for the first 200 years. A few other fission products, such as  $^{99}\text{Tc}$  and  $^{129}\text{I}$ , have very long half-lives, however the low concentration of these isotopes diminishes their overall importance to the waste hazard. Actinide materials such as  $^{241}\text{Am}$  and  $^{243}\text{Am}$  have even longer half-lives and dominate the waste hazard beyond 1000 years. The  $^{237}\text{Np}$  isotope has a half-life of 2 million years and its hazard dominates up to 20 million years before the  $^{238}\text{U}$  decay chain takes control. In contrast to the current strategy of permanent storage of spent fuel in a geological repository, the transmutation or burning of long-lived actinides by irradiation could be used as a method of ultimate disposal. Earlier studies<sup>1,2,3</sup> have shown that greater long-term safety could be achieved in the disposal of high-level wastes if actinides are separated from the fission products and burned in power reactors. If so, the actinides will be continuously recycled and will not be discharged to the environment until the reactor is shutdown.

Feasibility studies of actinide transmutation in power reactors have shown that Liquid Metal Fast Breeder Reactors (LMFBRs) offer an advantage because of a preferential fission to capture reaction ratio in the harder neutron spectrum<sup>4,5</sup> and a lower spontaneous fission neutron activity.<sup>6</sup> Research groups at General Electric<sup>7</sup>, Oak Ridge National Laboratory<sup>8</sup> and Combustion Engineering<sup>9</sup> have studied the actinide transmutation in LMFBRs using specially designed target fuels loaded at the central zone of the core so that the actinides are effectively burned in target zones while the actinide production and destruction are balanced in the rest of the core region at the equilibrium state. Beaman<sup>10</sup> used a typical 1200 MWe LMFBR and found that 113 kg of actinides, which is the amount of actinide from one LMFBR and three 1200 MWe Light Water Reactors (LWRs), are burned per cycle. Williams et al.<sup>8</sup> also

used a 1200 MWe LMFBR but elevated the specific power and core burnup by 15% from those of a commercial LMFBR. At the equilibrium state, the actinides from one LMFBR and one LWR can be consumed when target fuels are diluted 65% by  $^{238}\text{U}$  to prevent local power peaking in the target zone. These studies have shown that the physics characteristics of the system are not sensitive to the actinide target loading.

Robinson et al.<sup>11</sup> proposed a 1100 MWth Actinide Burner Reactor with a very hard spectrum determined by a sodium-to-fuel ratio of 1.01. Parametric studies were performed for core geometry (homogeneous and two-zone core), fuel composition, lattice arrangement, actinide fuel type, and the concentration of molybdenum diluent. This conceptual burner model could process two conventional 1100 MWe LWRs when optimized in a two-zone reactor. Balz et al.<sup>12</sup> have studied minor actinide burning in the European Fast Reactor. Parametric studies on the minor actinide content showed that the void worth increased too much when the minor actinide content exceeded 10% because the reactivity worth of  $^{237}\text{Np}$  and  $^{241}\text{Am}$  increases much more than the worth of  $^{238}\text{U}$  upon core voiding. On the other hand, the Doppler constant decreased too much when the minor actinide content exceeded the limiting value because resonance capture of  $^{237}\text{Np}$  and  $^{241}\text{Am}$  is less sensitive to temperature change than that of  $^{238}\text{U}$  which is the most dominant resonance absorption isotope in the commercial power plant. Due to limitations on the minor actinide content, the core design of Balz et al. can consume the minor actinide inventory of only 4 LWRs of the 1200 MWe type.

Japanese research groups are actively involved in transmutation analysis of minor actinides in fast reactor systems. Wakabayashi et al.<sup>13</sup> have studied a 1000 MWe LMFBR with a homogeneous loading of transuranic (TRU) nuclides. In the case of oxide fuel, the amount of TRU from six 1000 MWe LWRs, which is 5% of the total heavy metal loading, can be transmuted without any degradation of core performance. Hayase et al.<sup>14</sup> have used Mixed Oxide (MOX) fuel with a 10% enrichment of minor actinide in a 1000 MWe LMFBR. They could dispose of minor actinides from ten

1000 MWe LWRs per year with a 35% increase in the sodium void worth as a penalty compared to the core without minor actinide enrichment.

There has also been considerable research on metallic fuels because of the benefits of the harder neutron spectrum as well as the possibility of a more compact and economical fuel cycle. Mukaiyama et al.<sup>15</sup> have designed a Minor Actinide Burner (MAB) with two alloy fuels: Np-(Pu)-Zr and Am-Cm-(Pu)-Y. This MAB can burn the minor actinides from 12 typical 1000 MWe LWRs. Sasahara and Matsumura<sup>16</sup> have also used metallic fuel in a 1000 MWe LMFBR. Their core design consisted of two homogeneous zones; the plutonium enrichment is higher in the outer core to control the reactivity and power distribution. Their metal fuel burner is capable of transmuting TRUs produced from 18 1200 MWe LWRs. Hill et al.<sup>17</sup> have applied the Integral Fast Reactor (IFR)<sup>18</sup> concept to a 1200 MWth MAB design which was modeled homogeneously after a small change of fuel pin size. This MAB could burn minor actinides of twelve 1000 MWe LWRs. A similar study<sup>19</sup> by Rockwell International used a two-zone core concept for a 1160 MWth MAB. This MAB could burn minor actinides of 15 1000 MWe LWRs but the sodium void worth and reactivity burnup swing were estimated to be much higher than those of Hill's design.

The objective of this work is then to perform physics studies of a MAB design with a minor actinide inventory much greater than would be considered to be practical with current nuclear fuel technology and to determine if an acceptable core safety performance can be achieved. Specifically, this study will examine three of the most important safety performance parameters of a Liquid Metal Reactor (LMR); the burnup reactivity swing, the sodium void worth, and the Doppler constant.

## II. DESIGN MORPHOLOGY

In this section, design criteria used for MAB design are described. This section also includes descriptions of the cross-section data used for calculations and the closed fuel cycle model of MAB.

### II.1 Design Criteria

The neutronics design of a reactor core needs data from Thermal-Hydraulics (T/H) and material analysis. Because the properties of minor actinide fuels and the characteristics of the fuel assembly are not known at the beginning of design analysis, some of these parameters have to be assumed based on the similar core designs. The Sodium Advanced Fast Reactor (SAFR)<sup>20</sup> and Japanese Actinide Burning Reactor (ABR)<sup>21</sup> core models supply reasonable initial design data. The nominal design is the same as the IFR core, which is the updated version of the SAFR core: 91.44 cm (36 in.) of active fuel height, 0.724 cm (0.285 in.) of pin diameter, and 900 MWth of reactor power. These parameters are to change, depending on the performance of the MAB.

The fuel is composed of actinide material and 25% of zirconium. The theoretical density is assumed to be 75% to allow for fuel expansion and a high discharge burnup.<sup>20</sup> The fuel does not have an axial blanket in order to simplify the fabrication process. The design limit of the discharge burnup is 200 MWd/kg. There is no design limit for burnup reactivity swing and coolant void worth. But the absolute value of the burnup reactivity swing and the coolant void worth should be as small as possible satisfying other design limits. In this study, these are tentatively assumed to be  $\pm 1\% \delta k$ . The thermal conductivity of minor actinide alloy fuel is expected to be smaller than that of U-Pu-Zr alloy.<sup>21</sup> Comparing the values used for SAFR and ABR design, the thermal conductivity of 22 W/m<sup>o</sup>K is used for minor actinide alloy fuel. It is assumed that the pumping power is enough to maintain a coolant velocity of 6 m/sec.

The most crucial design criteria is the peak linear power because the fuel centerline temperature can not exceed the melting point (1160°C). The design limit of peak linear power for the IFR is 49.2 kW/m but the peak power density of IFR fuel (40.0 kW/m) is used here for the regular fuel pins in the MAB design in order to allow more thermal margin. The nominal design data and design limits are summarized in Table I.

## II.2 Cross-Section Data

The diffusion and depletion codes used in the work are DIF3D<sup>22</sup> and REBUS-3<sup>23</sup>, respectively, which require the cross-section data in the format of ISOTXS. The ANL research groups have generated 9-group ISOTXS set by processing ENDF/B-V for the analysis of an LMR such as SAFR and the IFR core. This 9-group cross-section set was used for all the depletion calculation of the MAB conceptual design as was done by the other study<sup>17</sup>. In addition, three 21-group cross-section sets were also generated to evaluate the void worth and Doppler constant for different reactor conditions such as flooded, voided, and hot core. The flooded core has normal temperature and coolant densities. In the voided core, the coolant which directly contacts the fuel rods is voided in the active core, upper plenum, and upper shield region. The coolant in the duct region and the non-fuel channel is assumed not to be voided because the voiding in these low power region is expected to be delayed compared with the fuel assembly. The hot core cross-section data were prepared by doubling the fuel temperature.

## II.3 Fuel Cycle Model

In the MAB, it is important to "close" the fuel cycle such that the minor actinides are not discharged to the environment throughout the reactor lifetime. Because the reprocessing and fabrication of minor actinide fuel has not been developed and demonstrated precisely, the following fuel cycle scenario is tentatively used for the

MAB fuel cycle.

### II.3.1 In-Core Fuel Cycle

It is practical to assume that a reactor is operated on a fixed fuel management scheme and maintains its criticality during normal operation. Under these conditions, the reactor condition is invariant for successive fuel cycles and this core is called a "k-constrained equilibrium core". The core can also be constrained with the discharge burnup, but only the k-constraint was used in the MAB design. The equilibrium core is found by adjusting the charge enrichment which is defined as the volume ratio of class 1 to class (1+2) fuels. Typically class 1 is defined as the more reactive materials by the users. The following equations describe the solution strategy.

$$\vec{n}_T = M(T, e, \vec{n}_c) \vec{n}_c \quad (1)$$

$$\vec{n}_c = Q_r(\vec{n}_T) \vec{n}_T + Q_f(\vec{n}_T) \vec{n}_f \quad (2)$$

$$k = k(T, e, \vec{n}_c) \quad (3)$$

In Eq.(1), the discharge number density vector ( $\vec{n}_T$ ) is determined by the transmutation matrix ( $M$ ) and initial number density vector ( $\vec{n}_c$ ). The transmutation matrix is expressed as a function of cycle length ( $T$ ), charge enrichment ( $e$ ), and charge density. Because the cross-section is an invariant quantity and the transmutation flux is a function of cross section and number density, they are not shown in Eq.(1). After each cycle, the charge density is re-calculated using the discharge density and external feed density ( $\vec{n}_f$ ) in Eq.(2). The discharged fuel is reprocessed and shuffled through the operator  $Q_r$ . The external feed material, which is LWR-discharged fuel in this study, is processed through the fabrication operator  $Q_f$ . If the k-constraint, which is expressed as a function

of cycle length, charge enrichment, and charge density in Eq.(3), is not satisfied either at Beginning of Equilibrium Cycle (BOEC) or End of Equilibrium Cycle (EOEC) state, the region-dependent charge density ( $e$ ) is linearly interpolated based on the previous estimate. The new charge density is calculated using the compositions of class 1 and 2 feed material obtained from Eq.(2). These procedures are continued until the constraint is satisfied and number densities are converged.

### *II.3.2 Ex-Core Fuel Cycle*

The MAB has two fuel sources: LWR and MAB discharged fuel. The LWR-discharged fuels are sent to the pyrochemical plant after a 3 year cooling time and reprocessed with MAB- discharged fuels which have been cooled for 2 years. In the pyroprocess, plutonium and uranium are collected on the cathodes with minor actinides.<sup>24</sup> Fission products and americium are not separated in this process and are sent to storage. But the recovery factors of fission product and americium are assumed to be 4% based on Ref.25 to allow for possible impurities during the reprocessing and further partitioning of minor actinides (e.g. <sup>237</sup>Np) is assumed to be done in the 2nd stage of the pyroprocess (post-reprocess). Total reprocessing time is assumed to be 6 months. After reprocessing, fuels are fabricated in the fabrication plant and excess plutonium will be sent to a Pu-burning core or to a storage facility. Therefore minor actinides, except americium which is not recovered in the pyroprocessing, are enclosed in a fuel cycle which is composed of a MAB and a reprocessing plant. The fabrication time is assumed to be 6 months. The overall mass flow is depicted in Fig.1. The isotopic composition of a typical LWR-discharged fuel is shown in Table II.

## **II.4 Safety Performance Parameters**

### *II.4.1 Burnup Reactivity Swing*

The burnup reactivity swing is defined as the difference of unpoisoned  $k_{eff}$  at BOEC

and EOEC state ( $\Delta k_{BU} = k_{BOEC} - k_{EOEC}$ ). The unpoisoned  $k_{eff}$  is the effective multiplication factor when the core does not have poison material such as burnable poison or control rods. It is desirable to minimize the  $|\Delta k_{BU}|$  because consequences of the control rod runout transient overpower (TOP) event can be minimized with near-zero  $\Delta k_{BU}$ .<sup>26</sup> If the core geometry and other parameters are fixed, the burnup swing depends on cycle length and fuel composition. The  $|\Delta k_{BU}|$  increases as the cycle length increases because the fissile material is destroyed or bred continuously during the fuel cycle. It is possible to reduce  $|\Delta k_{BU}|$  using a relatively short cycle length but this requires frequent reactor shutdown for refueling and the fuel economy becomes poor because of low discharge burnup. This problem can be resolved to a certain extent by incorporating a multi-batch core model which has an appropriate cycle length and number of batches.

#### II.4.2 Sodium Void Worth

The loss of sodium has a global effect of positive reactivity in most LMR cores due to several mechanisms<sup>27</sup>: spectral hardening, increase of neutron leakage, reduction in sodium capture, and change in self-shielding. If the sodium is lost, the neutron moderation is reduced and the spectrum hardens. The spectral hardening is the most dominant effect of positive void worth. If the coolant is voided, the neutrons have a greater probability to escape the core and this results in the negative effect on the void worth. Hitachi<sup>28</sup> proposed a core which is loaded with partial fuel on the upper boundary area such that the  $\delta D$  increases considerably on the boundary in the case of coolant voiding. The pancake type core has a large flux gradient and the void worth could be negative if the ratio of height to diameter (H/D) is very small ( $\sim 0.2$ ).<sup>29</sup> But the neutron economy of a high-leaking core is poor and requires more fissile material to compensate for the neutron losses. Therefore the burnup reactivity swing would be increased and the minor actinide transmutation will be reduced. The design options that can reduce the void worth will have tradeoffs for other performance parameters such as the burnup reactivity swing and minor actinide transmutation.



### *II.4.3 Doppler Constant ( $K_D$ )*

The Doppler constant is defined as the change in reactivity due to the relative variation of fuel temperature. The reactivity changes because the capture and fission resonances are broadened as the temperature increases (Doppler effect). In a typical fast reactor, the absorption in the region of well-separated resonances is much smaller compared to thermal reactor because the neutron spectrum is harder and the resonance peaks become flatter at higher neutron energy.<sup>30</sup> Due to the harder spectrum and the nature of resonances at high energy, the Doppler effect is dominant in the region of about 1 keV. It is important to keep the Doppler constant negative in order to have a prompt negative feedback from the prompt critical core in the case of a power transient because the control rod movement is slow after a prompt critical excursion. A relatively large part of the Doppler effect comes from fertile material,  $^{238}\text{U}$  or  $^{232}\text{Th}$ , due to their large increase in the effective parasitic capture cross-sections. In the MAB design,  $^{238}\text{U}$  is not fed to the core to prevent further higher actinide production. Because metallic fuel is used in the MAB, the spectrum is even harder and the magnitude of the Doppler constant will be very small. As far as Doppler constant is concerned in this study, a core model with a negative Doppler constant will be accepted regardless of its magnitude.

### III. HOMOGENEOUS MINOR ACTINIDE BURNER DESIGN

The presence of a substantial minor actinide inventory in the fuel poses some challenging core design problems. For example, the buildup of the highly reactive  $^{238}\text{Pu}$  from neutron capture in  $^{237}\text{Np}$  makes it difficult to maintain both a low burnup reactivity swing and a low sodium void worth. The effort to minimize the buildup of more transuranic isotopes during core operation discourages the use of fertile material<sup>31</sup> such as  $^{238}\text{U}$  and this causes a very small Doppler constant.

The homogeneous core model is preferable because it simplifies fuel fabrication and management. However, the void worth of homogeneous cores becomes unacceptably large (positive) as the minor actinide inventory is increased because of the fast fission effect of the minor actinides (e.g.  $^{237}\text{Np}$ ). On the other hand, if the fuel volume fraction is reduced in order to increase the core leakage and reduce the void worth, the burnup reactivity swing becomes unacceptably large and the minor actinide inventory is reduced. In general, the most important performance parameters (burnup reactivity swing, sodium void worth, and Doppler constant) can not be satisfied completely because the design changes that favor one parameter generally have a deleterious effect on the others.<sup>32</sup>

In the following sections, the assumptions used in MAB fuel cycle will be discussed and a parametric study will be performed for homogeneous core models. A homogeneous core was selected first as a base model for MAB design. The cycle length was studied to see the effect on the burnup reactivity swing. Fuel assembly design was studied by changing the pitch length and number of fuel pins. The effect of reactor power was studied too and finally the core geometry was altered to the pancake core and annular model.

### III.1 Base Minor Actinide Burner Model

As a first step, the MAB core was modeled homogeneously. In order to simplify the fuel fabrication, axial or internal blankets were not considered. The base core model was selected based on the IFR fuel design with a reactor power of 900 MWth. Several B<sub>4</sub>C blocks are deployed to reduce the possible power peaking in the central zone. The horizontal and vertical configurations of the base core model are shown in Figs.2 and 3, respectively. The radial boundary of the core is reflected and shielded with stainless steel and B<sub>4</sub>C blocks, respectively. The fuel assemblies have an active core height of 91.44 cm with a 15.4758 cm lattice pitch in the hexagonal array. In the fuel assemblies, a 30.48 cm thick lower axial shield is placed below a 50.8 cm thick lower plenum zone. Above the active core, there is a 127 cm thick upper plenum and a 30.48 cm thick axial shield. The plenum region is composed of sodium coolant and HT-9 structural material. The axial shield zone is filled with the coolant, structural material, and B<sub>4</sub>C absorber. The absorbing parts of the control assemblies are parked above the active core. The characteristics of the base core is given in Table III.

The charged fuel of the base core is composed of 90% minor actinides and a total of 877 kg of minor actinides are consumed every year. The most abundant material (40 wt% of charged fuel) in the core is <sup>237</sup>Np which through neutron capture becomes <sup>238</sup>Pu which is very reactive in a hard neutron spectrum. For example, the  $\eta$ 's of <sup>237</sup>Np and <sup>238</sup>Pu are 0.94 and 2.46, respectively, in this system. Therefore the transmutation of <sup>237</sup>Np and production of <sup>238</sup>Pu leads to a negative burnup swing (e.g. the core reactivity increases during the burnup cycle). The void worth is large and positive because most of the minor actinides have a fast fission-cross section at a higher energy region above 1 MeV. Most of the positive effect comes from the increased fast fission (due to spectrum hardening) of <sup>237</sup>Np which is most abundant in the base core. The leakage component is 5% of the total worth of the absolute value at BOEC. The void worth at EOEC is a little smaller because 14% of minor actinides are transmuted at the discharged state. In this study, the void worth and Doppler constant

were evaluated only at BOEC state for the homogeneous core models. The Doppler constant is very small at BOEC ( $K_D = -9.4 \times 10^{-5} T \delta k / \delta T$ ) and does not change much during the cycle. Because there is no strong resonance material, the Doppler effect comes from the most abundant material  $^{237}\text{Np}$ , which has its highest resolved resonance at 130 eV. The properties of the base core is summarized in Table IV.

### III.2 Effect of Fuel Cycle Length

The base core was run with two cycle lengths, 304 and 608 days, using a one-batch mode in which all the fuel is charged and discharged at the same time. Because the fuel residence time of the long cycle (608 days) is twice that of a short cycle (304 days), the minor actinide transmutation rate of the long cycle is almost twice of short cycle at the discharged state (EOEC). But the annual minor actinide consumption is about 6% higher in the short cycle model because the transmutation is not a linear function of time. The burnup reactivity swing is much higher (1.7%  $\delta k$ ) in magnitude for the long cycle model because more  $^{238}\text{Pu}$  is produced during the cycle.

The minor actinide consumption of the base core model, which has 2 batches, is about 4% lower than that of the short cycle model. But the burnup reactivity swing of the base core is almost the same as that of the short cycle model. The void worth and Doppler constant of these three models are close to each other. Although the short cycle model with a single-batch has an advantage in minor actinide consumption, the fuel fabrication effort will be doubled because all fuel assemblies are charged at the BOEC state while only half of the fuel assemblies are newly loaded in the base core model. Therefore the multi-batch core with the shorter cycle length has an advantage in burnup reactivity swing and fabrication cost reduction if the cycle length is not too short. The effect of the cycle length is summarized in Table V.

### III.3 Effect of Sodium Fraction and Core Size

#### III.3.1 Sodium Fraction

There are 271 fuel pins in the base core fuel assembly. The number of fuel pins was changed to 217, 169, and 91 which corresponds to the pin pitch length of 0.960, 1.097, and 1.537 cm. The core volume was increased radially (Figs.4-6) as the pitch length increased to conserve the total fuel volume and, therefore, the larger core has a larger sodium fraction. Other fuel cycle parameters are the same as the base core model. The increasing sodium fraction causes spectrum softening (Fig.7) and more neutron leakage. As the spectrum becomes softened, the core needs more fissile material to maintain the excess reactivity. Due to a lower minor actinide charge enrichment and softer spectrum, the minor actinide consumption is considerably deteriorated in the 8core with a large sodium fraction. The reactivity burnup reactivity swing changes from -2.06 to 2.83%  $\delta k$  as the sodium fraction changes from 0.36 to 0.73 because more fissile material is loaded as the sodium fraction increases.

The void worth increases as the sodium fraction increases up to about 0.6 and then decreases. The spectral and leakage component are proportional to the magnitude of the void perturbation and flux level. Because the variation of the perturbation and flux level are not a linear function of the sodium fraction, the void worth increases in the under-moderated region and decreases in the over-moderated region, which leaves a void worth peak at the intermediate region, as sodium fraction increases. The negative effect of the leakage component does not decrease the void worth until the assembly is mostly composed of sodium ( $\sim 70\%$ ) such that the axial leakage becomes dominant through both the voided channel and upper plenum.

As the spectrum shifts to the epithermal region, the Doppler effect becomes large. The Doppler constant for a high sodium fraction (0.73) assembly is about 2.7 times larger ( $-2.4 \times 10^{-4} T \delta k / \delta T$ ) than that of the base core ( $-9.4 \times 10^{-5} T \delta k / \delta T$ ) in

absolute value. The fuel composition also contributes to the Doppler constant.  $^{240}\text{Pu}$ , which has a large resonance at 2.4 keV, comprises 22.9% of the charge density for the core with a sodium fraction of 0.73 while it is only 0.75% for the base core. The effect of sodium fraction is summarized in Table VI.

### *III.3.2 Core Size for High Sodium Fraction Assembly*

The core with high sodium fraction (0.73) has 390 driver assemblies. This core was studied more closely to examine the effect of core size on neutron leakage. The reactor power was the same as the base core model (900 MWth) but the number of driver assemblies was reduced to 294 and 222. Because the same reactor power was used, the linear power and discharge burnup increased as the fuel inventory was reduced. It was assumed that the fuel pin could be split into smaller pins to reduce the fuel centerline temperature if the peak linear power exceeded the design limit.

Because the reactor power is the same, the peak fast flux of the 222-driver core is 1.6 times higher than that of the 390-driver core. Therefore the neutron leakage is high in the smaller core due to core size and flux level, and the reactivity loss is compensated by the high fissile charge enrichment. Because the fissile inventory is large ( $\sim 36$  wt%), the burnup reactivity swing is very high ( $7.1\% \delta k$ ), but the negative void worth was achieved at BOEC of the small core. The minor actinide consumption is poor in the small core because the core is mostly fed with plutonium. The characteristics of the small cores are compared in Table VII.

### **III.4 Effect of Moderating Material**

One way to prevent the spectrum hardening is to use scattering rods such that the neutron is still moderated even if the sodium is lost. The fuel assembly of a 390-driver core (Fig.6) was modified such that it contains 91 fuel pins and 180 BeO rods. The BeO rod has the same size as a regular fuel pin and therefore the coolant area of

the moderated assembly is the same as that of the base core assembly. In the 390-driver core, the replacement of BeO rods with sodium induced more spectrum softening (Fig.8) and therefore minor actinide consumption deteriorated. Though the burnup reactivity swing was increased by 0.56%  $\delta k$  from the unmoderated core (390-driver core without BeO rods), the sodium void worth was reduced to 0.53%  $\delta k$  at BOEC because the scattering cross-section was not perturbed much due to the scattering rods. If the HT-9 is used as a moderating material in the same core model, it was possible to reduce the void worth to 0.22%  $\delta k$  at BOEC, but there were tradeoffs in minor actinide consumption and burnup reactivity swing. The effect of scattering material is summarized in Table VIII.

### III.5 Effect of Reactor Power

Instead of changing reactor size, the reactor power was reduced to 600 and 330 MWth for which the number of drivers are 102 and 48, respectively, to keep the same power density. For the 330 MWth core, the void worth was reduced by 1.98%  $\delta k$  from the base core because the volume of the perturbed region is small in the spectral component of the void worth. The small core also has a greater leakage effect because the flux gradient is larger. Therefore more fissile is charged to the core and this changes the burnup reactivity swing to a positive value (0.38%  $\delta k$ ) and reduces the minor actinide consumption. The effect of reactor power is summarized in Table IX.

### III.6 Effect of Core Geometry

#### III.6.1 Reduced Core Height

The core height was reduced to 76.10 and 56.90 cm, which increased the number of drivers to 180 and 222, respectively, to maintain the same fuel volume. The characteristics of these cores are shown in Table X. The H/D ratio changed from 0.433 (base core) to 0.293 and 0.213 as the core height was reduced to 76.10 and 56.90

cm, respectively. Due to greater axial leakage in the smaller core ( $H=56.90$  cm), the charge enrichment was increased slightly and the burnup reactivity swing was changed toward positive direction. The minor actinide consumption was reduced by 7% in the smaller core because their charge fraction was reduced by the similar rate. The void worth was reduced by  $0.86\% \delta k$  for the smaller core because the flux gradient is larger on the top and bottom boundaries causing more neutron leakage, but the absolute value was still high ( $3.27\% \delta k$ ) and positive.

### *III.6.2 Annular Core Model*

The neutron leakage increases as the core surface area increases. The annular core was modeled by deploying several  $B_4C$  blocks in the central zone (Fig.9). The power peak in the central zone could also be avoided with this geometry. Both the inner and outer boundaries are reflected with stainless steel blocks and shielded with  $B_4C$  blocks. Three different models were studied as shown in Table XI.

The first model has the same number of drivers (138) as the base core and the control rods are all withdrawn like the base core. So the control rod sites are filled with sodium and duct material. Due to the increased leakage, the fissile charge was increased by 89% from the base core. Though this reduced the minor actinide consumption somewhat ( $\sim 5\%$ ), the burnup reactivity swing and void worth were reduced to  $-1.56$  and  $3.60\% \delta k$ , respectively. It was found that the peaking factor was changed from 1.55 to 1.46 as the model changed from the homogeneous base core to the annular core.

In the second model, the sodium of the control rod sites was replaced with HT-9 rods which have the same size as a  $B_4C$  control rod. In other words, the HT-9 rods are used as a parking portion of the control rod, and therefore the control sites are filled with HT-9 rods where the control rods are withdrawn. The neutron spectrum was not softened much because the HT-9 rods were sparsely distributed. Compared to the first model, the variation of performance parameters are small, about 4 and



7% reduction in minor actinide consumption and void worth, respectively.

In the last model, the sodium fraction of the driver was increased to 0.73 which is equivalent to an assembly with 91 regular fuel pins. The number of drivers was increased to 378. The control rod sites were filled with HT-9 rods again. As in Section III.C, the softened spectrum caused more fissile loading and a deterioration of the minor actinide consumption.

### III.7 Summary

Through the parametric study of homogeneous core models, it was found that the improvement in one performance parameter has drawbacks on other parameters. The minor actinide consumption depends on the amount of minor actinide material charged to the core which is determined by the neutron spectrum and leakage rate. The sodium fraction and scattering material have a considerable effect on the neutron spectrum. The neutron leakage depends on the core geometry and the sodium fraction in the fuel assembly. The minor actinide consumption is significantly deteriorates when the neutron spectrum is thermalized

The reactivity burnup swing changes from negative to positive as the fissile enrichment increases. Though a zero burnup swing is achievable without hurting the peak linear power, the void worth is still high and the minor actinide consumption is reduced because the minor actinide charge is decreased to accomodate  $^{238}\text{Pu}$  buildup, which is highly reactive in the MAB studied here.

In most cases, the void worth is larger than  $2\% \delta k$ . A negative void worth was obtained when the sodium fraction was large (0.73) and the power density is high such as a small core (222- driver core). Because the leakage becomes high in this core, the burnup reactivity swing and the minor actinide consumption deteriorate. A small void worth is achievable using scattering material which prevents spectrum hardening to a certain

extent, but the burnup reactivity swing and the minor actinide consumption are further reduced.

The annular core model has an advantage to reduce the power peaking compared to the pancake type core without significantly deteriorating the burnup reactivity swing and the minor actinide consumption. Further void worth reduction is achievable by deploying scattering material (e.g. HT-9) in the control rod sites.

#### IV. DECOUPLED MINOR ACTINIDE BURNER DESIGN

The homogeneous core models have difficulty in simultaneously satisfying the MAB performance requirements of a massive minor actinide consumption rate, a low burnup reactivity swing, and a low void worth. In this section, results are reported for modeling the core with two different zones (decoupled core); a minor actinide zone and plutonium enriched zone. The minor actinide zone was used to burn the minor actinides effectively using a hard spectrum while the plutonium zone was introduced to compensate for the deteriorating safety performance due to heavy minor actinide loading. The decoupled core was modeled in annular geometry with HT-9 rods in control rod sites to prevent further spectrum hardening in the case of coolant voiding. After trying several models, a decoupled core was selected as the base model. In the following sections, the property of the base core will be discussed. A comparative study will be done for the cores which have different characteristics.

##### IV.1 Base Decoupled Core

The base decoupled core has the same power (900 MWth) and core height (91.44 cm) as the homogeneous base core. The fuel cycle length is the same (304 days) but the number of batches was increased to three in order to increase the discharge burnup. There are 114 driver assemblies in both the inner and outer core zone. The sodium fraction of the inner and outer core assembly is 0.36 and 0.73, respectively, which corresponds to 271 and 91 regular fuel pins per assembly, respectively. The sodium fraction in the outer core is larger to cause more neutron leakage. The minor actinide and plutonium fuels are loaded in the inner and outer core zone, respectively. The characteristics and configuration of the base decoupled core is shown in Table XII and Fig.10, respectively. The compositions of the inner and outer core fuel are given in Table XIII.

Compared to the results of the homogeneous base core, both the burnup reactivity

swing and the void worth were improved in the decoupled core but the minor actinide consumption was decreased by 189 kg/yr. The burnup reactivity swing became relatively small ( $0.78\% \delta k$ ) because the  $^{238}\text{Pu}$  buildup from the neutron capture of  $^{237}\text{Np}$  was compensated by the fissile ( $^{239}\text{Pu}$  and  $^{241}\text{Pu}$ ) burning in the outer core. The sodium void worth was reduced to  $1.3\% \delta k$  at the BOEC state. The spectrum hardening caused more neutron production in the inner core but the production rate in the outer core decreased more than the absorption rate because the total flux level decreased to compensate for the power increase in the inner core. Therefore it was possible to achieve a smaller void worth in the decoupled core.

#### IV.2 Effect of Moderating Material

The outer core driver of the base decoupled core was changed to have 78 and 180 BeO rods in the medium moderated and highly moderated cores, respectively, to soften the spectrum in this region. The moderating pin has the same size as the regular fuel pin. Therefore the sodium coolant area of the highly moderated core is the same in both the inner and outer core assemblies because there are 91 plutonium fuel pins of regular size. The core configuration is the same as the base decoupled core.

As the number of moderating pins increases, the burnup reactivity swing increases because more fissile plutonium is burned. The void worth was reduced by the use of moderating pins which prevent the spectrum hardening somewhat upon coolant voiding. The Doppler constant increases also in magnitude because the spectrum shifts towards the resolved resonance region where the Doppler effect is dominant.

For the highly moderated core, the burnup reactivity swing increases to  $3.7\% \delta k$ . The minor actinide consumption was reduced by 59 kg/yr compared to the base decoupled core. The void worth was reduced to  $0.47\% \delta k$  at BOEC state but the linear power of the outer core fuel pin was increased to 70 kW/m. The characteristics of the moderated core is shown in Table XIV. Though the moderated core has an advantage

in the void worth, it is doubtful if the moderated core would be attractive because of the large burnup reactivity swing and high linear power.

### IV.3 Effect of Outer Core Size

The number of assemblies in the outer core was increased from 114 (base decoupled core model) to 138 and 210 in the medium size and large size cores, respectively. There are 66 control rod sites in both the medium and large size cores while the base decoupled core has 42 control rod sites which are filled with the HT-9 rods. As the outer core size increases, the burnup reactivity swing increases. More fissile plutonium is transmuted in the outer core but the minor actinide consumption is decreased because the power level is reduced in the inner core. The minor actinide consumption was decreased by 28 and 36 kg/yr for the medium and large size cores, respectively, compared to the base decoupled core.

The void worth is smaller in the medium size core ( $1.05\% \delta k$  at EOEC) while it is larger ( $1.62\% \delta k$  at EOEC) for the large size core. The Doppler constants are not much different in each core model. The medium size core shows the better performance in the void worth though the burnup reactivity swing and the minor actinide consumption are slightly reduced. In the medium size core, the peak linear power of the inner core pin has sufficient margin and the discharge burnup is still below the design limit (200 MWd/kg). Therefore, it was decided to elevate the reactor power in the final core model such that the minor actinide consumption could be increased and to use a smaller fuel pin in the outer core to prevent a large temperature rise in the pin. The properties of these cores are compared in Table XV.

## V. FINAL CORE MODEL

The final core consists of 114 inner core assemblies (minor actinide fuel), 138 outer core assemblies (plutonium fuel), and 66 control rod sites (same as the medium size core model in Section IV.C). But the reactor power was set at 1200 MWth to increase the minor actinide consumption. Both the inner and outer boundaries are surrounded with stainless steel reflector and shielded with B<sub>4</sub>C blocks. The control rod sites are filled with HT-9 rods when control rods are not inserted in order to reduce the spectrum hardening in the event of coolant voiding. The upper and lower plenum region are composed of HT-9 structural material and sodium coolant. The upper and lower shields are placed next to the plenum region. The thickness of the plenum and shield are the same as those of the homogeneous base core model. The horizontal and vertical configurations of the core are shown in Figs.11 and 12, respectively.

The minor actinide and plutonium fuel assemblies have 271 and 162 fuel pins, respectively. The fuel has 25% zirconium and the theoretical density was assumed to be 75% to allow for fuel expansion and high discharge burnup. The isotopic compositions of the inner and outer core assemblies were determined using the equilibrium cycle capability of the REBUS-3 code. The inner core fuel is composed of 70% <sup>237</sup>Np and the outer core fuel is enriched to 50% with fissile plutonium. The plutonium fuel pin diameter is smaller to reduce the fuel center temperature. Because the outer core fuel is highly enriched and the inner core contains fertile <sup>237</sup>Np, the power shifts from the outer to the inner core during the cycle. The general core characteristics and fuel assembly data are summarized in Tables XVI and XVII, and the fuel composition is shown in Table XVIII. The equilibrium cycle performance parameters are given in Table XIX.

### V.1 Fuel Cycle

The minor actinide burner is operated with three fuel batches and a 10 month cycle

length. The relatively short cycle length is used to maintain an acceptable burnup reactivity swing. The feed material for the minor actinide burner is assumed to be from a typical 1000 MWe LWR after 3 years cooling. At the completion of each burnup cycle, the discharged fuel is recovered and fabricated with external feed material in the fabrication plant. The external feed material is assumed to be provided as separate plutonium and minor actinide streams with the isotopic distributions shown in Table II.

The minor actinide burner accepts 689 kg of minor actinides and 557 kg of plutonium per year. The minor actinides are continuously recycled in the core, however 70% of the fissile plutonium is surplus material and is assumed to be used as fissile makeup in other plutonium burning reactors. Considering 96% of the discharged americium which is not recovered in the reprocessing plant, the net consumption rate of minor actinides is 425 kg/yr. Assuming the typical 1000 MWe LWR generates about 26 kgs of minor actinides each year, the core design here can transmute the annual minor actinide inventory from about 16 LWRs.

## V.2 Safety Performance Parameters

The reactivity of the inner core will increase substantially with burnup, since the minor actinides fuel consists mostly of  $^{237}\text{Np}$  ( $\eta = 0.94$ ) which results in  $^{238}\text{Pu}$  ( $\eta = 2.46$ ) after a neutron capture. As the fuel depletes, this reactivity gain is compensated by the decrease in the fissile plutonium inventory in the outer core, resulting in a small positive burnup reactivity swing (1.19%  $\delta k$ ).

The dominant contribution to the sodium void worth is spectral hardening (Figs.13 and 14) which is mitigated to some extent by using the HT-9 rods in the control rod sites. The isotope most responsible for the increase in reactivity upon coolant voiding is  $^{237}\text{Np}$  for which  $\eta$  changes from 0.94 to 1.09 as the power level increases in the inner core. However, as the coolant voids in the outer core the neutron leakage increases

because the spectrum hardens and the neutron mean free path increases. The spectral hardening causes power reduction in the outer core while it increases the power in the inner core because of increased fast fission. Because the outer core is predominantly fissile material, a decrease in the power reduces the neutron production rate more than the absorption rate, which provides a negative coolant void worth in this region. Because the positive reactivity effect of the inner core dominates, the net effect is still a small positive void worth, however it is comparable to void worths allowed in conventional LMR designs.

Because the actinide burner does not contain  $^{238}\text{U}$ , the Doppler effect is smaller than a conventional LMR, but remains negative ( $-0.32 \times 10^{-3} T \delta k / \delta T$ ). At the EOEC, the core contains about 50%  $^{237}\text{Np}$  and therefore the largest contribution to the Doppler effect is from  $^{237}\text{Np}$  even though its highest resolved resonance is at 130 eV. The  $^{240}\text{Pu}$  and  $^{242}\text{Pu}$  have their strong resolved resonances at about 2.4 and 0.9 keV, respectively, but their contribution to the Doppler reactivity is small since they comprise only 6.8 and 1.4% of the EOEC loading, respectively. The safety performance parameters are summarized in Table XX for both the BOEC and the EOEC core conditions.

### V.3 Estimation of Fuel Temperature

The ultimate safety of the reactor core is the fuel integrity in case of transient overpower. Though the material and thermal property of the minor actinide and plutonium fuel is not yet known, it is worthwhile to estimate the fuel temperature using currently available or assumed data because the fuel temperature must not exceed the melting point. The thermal conductivity of the fuel is assumed to be 22 W/m<sup>o</sup>K based on SAFR and Japanese ABR designs. The specific heat and velocity of sodium coolant are 1.3 kJ/kg<sup>o</sup>C and 6 m/sec, respectively, based on Ref.27 and ABR design. The bulk coolant temperature is assumed to be 650<sup>o</sup>K. The sodium density and thermal conductivity are obtained using the following relations.



$$\rho(\text{kg/m}^3) = 1011.8 - 0.22054 T - 1.9226 \times 10^{-5} T^2 + 5.6371 \times 10^{-9} T^3 \quad (4)$$

$$k(\text{W/m}^{\circ}\text{K}) = 93.0 - 0.0581 (T - 273) + 1.173 \times 10^{-5} (T - 273)^2 \quad (5)$$

where  $T$  is temperature in degree Kelvins. The cladding temperature was assumed to be  $750^{\circ}\text{K}$  for the initial calculation. The thermal conductivity of clad material was obtained using the relation of 316 stainless steel as below,

$$k(\text{W/m}^{\circ}\text{K}) = 9.248 + 0.01571 T \quad (6)$$

where  $T$  is temperature in degree Kelvins. The calculated and assumed thermal properties are summarized in Table XXI.

### V.3.1 Inner Core Fuel Pin

The inner core assembly has 271 regular fuel pins of which the outer diameter, clad thickness, and pin pitch are 0.724, 0.056, and 0.853 cm, respectively. Using these values, the  $P/D$ , flow area ( $A$ ), wetted perimeter ( $P_w$ ), and effective hydraulic diameter ( $De$ ) of a subchannel were calculated, which are 1.18, 0.1098 cm<sup>2</sup>, 1.1379 cm, and 0.3855 cm, respectively. Then, the Peclet number ( $Pe$ ) was calculated to be 356 and the Nusselt number ( $Nu$ ) was obtained as 7.53 using Borishanskii-Gotovskii-Firsova (B-G-F) correlation<sup>33</sup> which is applicable for  $1.1 \leq P/D \leq 1.5$  and  $200 \leq Pe \leq 2000$ . Finally the heat transfer coefficient was calculated from another formulation for the Nusselt number.

$$h = Nu \frac{k}{D_e} = 142,000 \text{ W/m}^2\text{K} \quad (7)$$

The position of the maximum fuel-center temperature along the fuel element is obtained

using the equations in Ref.34. The maximum coolant temperature rise was 24°K and, therefore, the maximum coolant temperature at the peak position is 654°K when the inlet temperature is 630°K. The temperature rise between bulk coolant and the fuel-center was 225°K, which resulted in the fuel-center temperature of 879°K (606°C). If there is a 115 % overpower, the coolant temperature rise will be 28°K and the maximum coolant temperature is 658°K. Then, the fuel-center temperature will be 917°K (644°C) which is considerably below the melting point (1160°C).

### *V.3.2 Outer Core Fuel Pin*

The final core model has 162 fuel pins in an outer core assembly with reduced pin size. For comparison, the fuel temperature was calculated for three different number of fuel pins; 91, 127, and 162 of which the pin size are 0.724, 0.612, and 0.544 cm. Therefore the material volumes of fuel, clad, and coolant are conserved in the three models such that the neutronic calculation won't be affected. The Graber and Rieger's correlation<sup>27</sup> was used to determine the Nusselt number for the range of  $1.25 \leq P/D \leq 1.95$  and  $150 \leq Pe \leq 3000$ . The fuel temperatures are listed in Table XXII with other parameters. For the assembly with 162 fuel pins, the centerline temperature was 640°C. In the case of 115% overpower transient, the fuel temperature increases to 683 °C and there is still 41% margin for fuel melting.

## **V.4 Summary**

A minor actinide burner was designed using several parametric studies. For the homogeneous core models, the void worth becomes unacceptably large (positive) as the minor actinide inventory is increased because of the fast fission effect of the minor actinides (e.g. <sup>237</sup>Np). On the other hand, if the fuel volume fraction is reduced in order to increase the core leakage and reduce the void worth, the reactivity burnup swing becomes unacceptably large and the minor actinide inventory is reduced.

One of the principal innovations used in the conceptual MAB design is to maintain a homogeneous core layout, but employ two core zones; an inner core consisting of minor actinide fuel and an outer core containing plutonium fuel. The plutonium outer core offsets much of the poor core safety performance caused by the presence of minor actinides in the inner core. The HT-9 rods are employed in the control rod sites as a means of further reducing the sodium void worth.

The final MAB model can consume the annual minor actinide waste from about 16 commercial Light Water Reactors (LWR). Because of the decoupled core design innovation, it was possible to maintain acceptable safety performance as indicated by the small burnup reactivity swing, the low sodium void worth, and the negative doppler constant. The fuel temperature was also kept below the melting point both in the inner and outer core.

## VI. SUMMARY, CONCLUSIONS, AND RECOMMENDATIONS

The feasibility of using minor actinides as fuel material in a LMR in order to reduce the long-term hazard due to the minor actinides discharged from an LWR has been studied in the work here. The principal problem of designing a minor actinide burning reactor is the difficulty in maintaining a small burnup reactivity swing and void worth, while maximizing the minor actinide consumption rate. In the case of a homogeneous core model, it was found that the burnup reactivity swing becomes large when the void worth is reduced because of a large increase in the neutron leakage. The minor actinide consumption rate also deteriorates because the core is primarily charged with fissile material in order to compensate for the reactivity loss due to the increased neutron leakage.

A conceptual design of the minor actinide burner has been performed using several parametric studies to maximize the consumption of minor actinides discharged from the LWR. The design effort was focused on reducing the burnup reactivity swing and coolant void worth, while keeping the Doppler constant negative. The core was designed in an annular decoupled model in which the minor actinides are transmuted in the inner core surrounded by the plutonium outer core to compensate for the deleterious effect of the minor actinides on the core safety performance.

The reactivity increases in the inner core zone during the cycle because the neutron capture of  $^{237}\text{Np}$  produces  $^{238}\text{Pu}$  which is more reactive in the minor actinide burner. The reactivity gain in the inner core is compensated by the fissile burning in the outer core. Because the reactivity loss is higher in the outer core, the burnup reactivity swing is positive and small ( $1.17\% \delta k$ ).

The void worth becomes positive and large in the inner core because the minor actinides such as  $^{237}\text{Np}$  undergo more fast fission when the neutron spectrum is hardened. Because of the increased fast fission in the inner core, the power level in the outer core is

reduced. Due to the nuclear properties of the fissile material loaded in the outer core, the production rate is reduced considerably in the outer core resulting in a small void worth for the entire core (1.19%  $\delta k$  at EOEC).

The Doppler constant was very small ( $-0.32 \times 10^{-3} T \delta k / \delta T$ ) because the fertile material such as  $^{238}\text{U}$  was not supplied from an external source to prevent further minor actinide production. By adopting the annular decoupled core model, it was possible to consume 425 kg of minor actinide per year which is equivalent to the minor actinides discharged from 16 1000 MWe LWRs.

As a recommendation, more research is required in the following areas:

- The feasibility of minor actinide burning is strongly dependent on the demonstration of fuel reprocessing and refabrication techniques. This should be a high priority for minor actinide burning research.
- The disposition of the excess plutonium produced from the minor actinide burner was not considered in this work. Though the plutonium can be used in several reactor types, it would be worthwhile to perform a detailed study in conjunction with the minor actinide burner research.

REFERENCES

1. H. C. Claiborne, "Neutron-Induced Transmutation of High-Level Radioactive Waste", ORNL-TM-3964, 1972.
2. A. S. Kubo and D. J. Rose, "Disposal of Nuclear Waste", *Science*, **182**, 1205, 1973.
3. J. W. Bartlett et al., "High-Level Radioactive Waste Management Alternatives, Section 7: Waste Partitioning", BNWL-1900, Battelle Pacific Northwest Labs., 1974.
4. R. J. Breen, "Elimination of Actinides with LMFBR Recycle", *Trans. of Am. Nucl. Soc.*, Vol.21, New Orleans, Louisiana, 1975.
5. T. H. Pigford and J. S. Choi, "Actinide Transmutation in Fission Reactors", *Trans. of Am. Nucl. Soc.*, Vol.27, San Francisco, CA, 1977.
6. A. G. Croff, "Parametric Studies Concerning Actinide Transmutation in Power Reactors", *Trans. of Am. Nucl. Soc.*, Vol.22, San Francisco, CA, 1975.
7. S. L. Beaman, "Actinide Recycle in LMFBRs as a Waste Management Alternative", *Trans. Am. Nucl. Soc.*, Vol.22, San Fransisco, CA, 1975.
8. M. L. Williams et al., "Preliminary Neutronic Study of Actinide Transmutation in a Fast Reactor", ORNL/TM-6309, 1978.
9. J. J. Prabulos, "Actinide Destruction in a 1500 MW(e) Carbide-Fueled LMFBR", *Trans. of Am. Nucl. Soc.*, Vol.23, Toronto, Canada, 1976.
10. S. L. Beaman and E. A. Aitken, "Feasibility Studies of Actinide Recycle in LMFBRs as a Waste Management Alternative", *Trans. of Am. Nucl. Soc.*, Vol.23, Toronto,

Canada, 1976.

11. A. H. Robinson et al., "Burning Actinides in Very Hard Spectrum Reactors", *Trans. of Am. Nucl. Soc.*, Vol.30, Washington D.C., 1978.
12. W. Balz et al., "Core Design and Safety Aspects of Large LMFBRs with Minor Actinide Recycling", International Fast Reactor Safety Meeting, Vol.I, 1990.
13. T. Wakabayashi et al., "Status of Study on TRU Transmutation in LMFBRs", *Trans. of Am. Nucl. Soc.*, Vol.64, San Francisco, CA, 1991.
14. T. Hayase et al., "Core Design Study for Actinide Burning LMFBRs", International Conference on the Physics of Reactors: Operation, Design and Consumption, Vol.4, Marseille, France, 1990.
15. T. Mukaiyama et al., "Minor Actinide Transmutation in Minor Actinide Burner Reactors", *Trans. of Am. Nucl. Soc.*, Vol.64, San Francisco, CA, 1991.
16. A. Sasahara and T. Matsumura, "An Assessment of TRU Recycling Transmutation in Metal Fuel FBR", International Conference on the Physics of Reactors: Operation, Design and Consumption, Vol.4, Marseille, France, 1990.
17. R. N. Hill et al., "Physics Studies of Higher Actinide Consumption in an LMR", International Conference on the Physics of Reactors: Operation, Design and Consumption, Vol.1, Marseille, France, 1990.
18. D. C. Wade and Y. I. Chang, "The Integral Fast Reactor Concept : Physics of Operation and Safety", *Nucl. Sci. Eng.*, **100**, p507, 1988.
19. Rockwell International, "Characteristics of a Minor Actinide Fueled Reactor", Proc.

- of Transmutation Workshop of the FFTF Internationalization Symposium, WHC-MR-0262, Westinghouse Hanford Company, 1991.
20. Y. Orechwa et al., "Core Design and Performance of Small Inherently Safe LMR's", Proc. of the Topical Meeting on Advances in Fuel Management, Pinehurst, NC, March 2-5, 1986.
  21. T. Mukaiyama, "Actinide Burner Reactor for Minor Actinide Transmutation: Design Study and Integral Experiment for Nuclear Fuel Material Evaluation", Proc. Transmutation Workshop of the FFTF Internationalization Symposium, WHC-MR-0262, 1991.
  22. K. L. Derstine, "DIF3D: A Code to Solve One-, Two-, Three-Dimensional Finite-Difference Diffusion Theory Problems", ANL-82-64, Argonne National Laboratory, 1984.
  23. B. Toppel, "A Users Guide for the REBUS-3 Fuel Cycle Analysis Capability", ANL-83-2, Argonne National Laboratory, Argonne, Ill., 1983.
  24. L. Burris et al., "A Proposed Pyrometallurgical Process for Rapid Recycle of Discharged Fuel Materials from the Integral Fast Reactor", Proceedings of Fuel Reprocessing and Waste Management Mtg., Vol.II, Jackson, WY, 1984.
  25. R. N. Hill, "Physics Studies of Higher Actinide Consumption in an LMR", Intra-Laboratory Memorandum, Applied Physics Division, Argonne National Laboratory, Sept. 2, 1988.
  26. T. Hamid, "Study of a New Compact Fast Reactor Core Design", Ph.D Thesis, School of Nuclear Engineering, Purdue University, 1990.



27. A. E. Waltar and A. B. Reynolds, *Fast Breeder Reactors*, Pergamon Press, New York, NY, 1981.
28. Hitachi, Ltd., "Decrease of Sodium Void Reactivity of Large Mox FBR Cores", Presented at Argonne National Laboratory, FN-ENZ-528, 1991.
29. R. N. Hill et al., "Calculational Benchmark Comparisons for a Low Sodium Void Worth Actinide Burner Core Design", Topical Meeting on Advances in Reactor Physics, Charleston, SC, 1992.
30. S. Glasstone and A. Sesonske, *Nuclear Reactor Engineering*, Van Nostrand Reinhold Company, New York, NY, 1981.
31. H. Kusters and H. W. Wiese, "Burning of Actinides and Fission Products in Reactors and Accelerator-Driven Spallation Sources", *Trans. of Am. Nucl. Soc.*, Vol.64, San Francisco, CA, 1991.
32. H. S. Khalil and R. N. Hill, "An Evaluation of Liquid Metal Reactor Design Options for Reduction of Sodium Void Worth", *Nucl. Sci. Eng.*, **109**, p.221, 1991.
33. V. M. Borishanskii et al., "Heat Transfer to Liquid Metal Flowing Longitudinally in Wetted Bundles of Rods", *Soviet Atomic Energy*, **27**, p.1347, 1969.
34. M. M. El-Wakil, *Nuclear Heat Transport*, International Textbook Co., Scranton, PA, 1971.

Table I  
Nominal Design Parameters of MAB

Reactor power (MWth)	900
Active core height (cm)	91.44
Fuel design	
Material type	MA/Pu+25%Zr alloy
Theoretical density (%)	75
Discharge burnup (MWd/kg)	200
Cooling time (yrs)	
LWR-discharged fuel	3
MAB-discharged fuel	2
Reprocessing time (month)	6
Refabrication time (month)	6
Recovery factors	
U/Pu/MA	1.00
Am & fission product	0.04

Table II  
Isotopic Composition of Discharged Fuel from 1000 MWe LWR  
after 3 Years Cooling

Class 1*		Class 2 <sup>+</sup>	
<sup>236</sup> Pu	$1.26 \times 10^{-7}$	<sup>237</sup> Np	0.491
<sup>238</sup> Pu	$1.14 \times 10^{-2}$	<sup>241</sup> Am	0.227
<sup>239</sup> Pu	0.571	<sup>242m</sup> Am	$1.00 \times 10^{-3}$
<sup>240</sup> Pu	0.224	<sup>243</sup> Am	0.225
<sup>241</sup> Pu	0.151	<sup>242</sup> Cm	$8.81 \times 10^{-5}$
<sup>242</sup> Pu	$4.36 \times 10^{-2}$	<sup>243</sup> Cm	$7.12 \times 10^{-4}$
		<sup>244</sup> Cm	$5.00 \times 10^{-2}$
		<sup>245</sup> Cm	$4.60 \times 10^{-3}$
		<sup>246</sup> Cm	$5.72 \times 10^{-4}$

\*Class 1 is the more reactive isotope group

<sup>+</sup>Class 2 is the less reactive isotope group

Table III  
 Characteristics of Homogeneous Base Core

Reactor concept	Homogeneous
Reactor power (MWth)	900
Active core height (cm)	91.44
Number of drivers	138
Number of control rod site	24
Number of B <sub>4</sub> C block	7
Fuel cycle	
Capacity factor (%)	80
Cycle length (days)	304
Fuel residence time (batch)	2
Fuel data	
Mass ratio (U/Pu/Np/Am/Cm)	4/5/72/11/8
Fuel pin outer diameter (cm)	0.724
Clad thickness (cm)	0.056

Table IV  
 Characteristics of Homogeneous Base Core

Minor actinide consumption (kg/yr)	878
Burnup reactivity swing (% $\delta k$ )	-2.1
Breeding ratio	1.18
Discharge burnup (MWd/kg)	67
Peak linear power (kW/m)	40.3
Peak flux ( $10^{15}$ n/cm <sup>2</sup> sec)	3.5
Peak fast flux ( $10^{15}$ n/cm <sup>2</sup> sec)	2.8
Charge enrichment (wt%)	
Minor actinide	90.3
Pu-fissile	0.3
Coolant void worth (% $\delta k$ )	
BOEC	4.1
EOEC	4.0
Doppler constant ( $10^{-4}$ T $\delta k / \delta T$ )	
BOEC	-0.94
EOEC	-0.94

Table V  
Effect of Cycle Length

	BASE	CY304	CY608
Power (MWth)	900	900	900
Cycle length (days)	304	304	608
Number of batches	2	1	1
Number of drivers	138	138	138
Actinide consumption (kg/yr)			
Pu-fissile	-12	-12	-13
Pu-total	-252	-246	-238
Minor actinide	531	527	518
Reactivity worth (BOEC)			
Burnup swing (% $\delta k$ )	-2.1	-2.0	3.8
Void worth (% $\delta k$ )	4.1	4.2	4.2
Doppler ( $10^{-4}$ T $\delta k / \delta T$ )	-0.94	-0.90	-0.91

Table VI  
Effect of Sodium Fraction

	BASE	SF5	SF6	SF7
Power (MWth)	900	900	900	900
Cycle length (days)	304	304	304	304
Number of batches	2	2	2	2
Number of drivers	138	174	222	390
Fuel pin pitch (cm)	0.853	0.960	1.097	1.537
Fuel pins per assembly	271	217	169	91
Fuel fraction (100% T.D.)	0.385	0.308	0.240	0.129
Structure fraction	0.256	0.223	0.193	0.144
Sodium fraction	0.359	0.469	0.567	0.727
Actinide consumption (kg/yr)				
Pu-fissile	-12	-14	-13	117
Pu-total	-252	-226	-113	162
Minor actinide	531	505	394	133
Reactivity worth (BOEC)				
Burnup swing (% $\delta k$ )	-2.1	-1.7	-0.4	2.8
Void worth (% $\delta k$ )	4.1	6.1	7.3	3.3
Doppler ( $10^{-4} T \delta k / \delta T$ )	-0.94	-0.98	-0.50	-2.40

Table VII

Effect of Core Size for High Sodium Fraction (0.727) Core

	SF7	SF7M	SF7S
Power (MWth)	900	900	900
Cycle length (days)	304	304	304
Number of batches	2	2	2
Number of drivers	390	294	222
Actinide consumption (kg/yr)			
Pu-fissile	117	144	192
Pu-total	162	200	267
Minor actinide	133	95	31
Reactivity worth (BOEC)			
Burnup swing (% $\delta k$ )	2.8	4.4	7.1
Void worth (% $\delta k$ )	3.3	1.5	-2.0
Doppler ( $10^{-4} T \delta k / \delta T$ )	-2.4	-3.4	-6.1



Table VIII  
Effect of Moderating Pins\*

	SF7	SF7BE	SF7HT
Power (MWth)	900	900	900
Cycle length (days)	304	304	304
Number of batches	2	2	2
Number of drivers	390	390	390
Moderating material	-	BeO	HT-9
Actinide consumption (kg/yr)			
Pu-fissile	117	169	167
Pu-total	162	235	232
Minor actinide	133	67	68
Reactivity worth (BOEC)			
Burnup swing (% $\delta k$ )	2.8	3.4	3.9
Void worth (% $\delta k$ )	3.3	0.5	0.2
Doppler ( $10^{-3} T \delta k / \delta T$ )	-2.4	-3.9	-0.5

\* 91 regular fuel pins + 180 moderating pins per assembly

Table IX  
Effect of Reactor Power and Size

	BASE	P600	P330
Power (MWth)	900	600	330
Cycle length (days)	304	304	304
Number of batches	2	2	2
Number of drivers	138	102	48
Actinide consumption (kg/yr)			
Pu-fissile	-12	-8	-4
Pu-total	-252	-169	-33
Minor actinide	531	355	136
Reactivity worth (BOEC)			
Burnup swing (% $\delta k$ )	-2.1	-1.8	0.38
Void worth (% $\delta k$ )	4.1	3.9	2.2
Doppler ( $10^{-4} T \delta k / \delta T$ )	-0.94	-0.93	-0.60

Table X  
Effect of Core Height

	BASE	PAN70	PAN57
Power (MWth)	900	900	900
Cycle length (days)	304	304	304
Number of batches	2	2	2
Number of drivers	138	180	222
Core height (cm)	91.44	70.10	56.84
H/D ratio	0.433	0.293	0.213
Actinide consumption (kg/yr)			
Pu-fissile	-12	-13	-14
Pu-total	-252	-239	-213
Minor actinide	531	518	492
Reactivity worth (BOEC)			
Burnup swing (% $\delta k$ )	-2.1	-1.9	-1.5
Void worth (% $\delta k$ )	4.1	3.8	3.3
Doppler ( $10^{-4}T \delta k / \delta T$ )	-0.94	-1.06	-1.13

Table XI  
Effect of Annular Geometry

	ANN1	ANN2	ANN3
Power (MWth)	900	900	900
Cycle length (days)	304	304	304
Number of batches	2	3	3
Number of drivers	138	138	378
Fuel rods per assembly	271	271	91
Control rod site	Sodium	HT-9	HT-9
Actinide consumption (kg/yr)			
Pu-fissile	-13	-14	124
Pu-total	-222	-205	172
Minor actinide	502	484	118
Reactivity worth (BOEC)			
Burnup swing (% $\delta k$ )	-1.6	-1.4	3.1
Void worth (% $\delta k$ )	3.6	3.4	1.8
Doppler ( $10^{-4} T \delta k / \delta T$ )	-1.0	-1.0	-4.6

Table XII  
 Characteristics of Decoupled Base Core

Reactor concept	Decoupled annular
Reactor power (MWth)	900
Active core height (cm)	91.44
Breeding ratio	0.15
Number of drivers	
Inner core	114
Outer core	114
Fuel pins per assembly	
Inner core	271
Outer core	91
Fuel mass ratio	
Inner core(U/Np/Am/Cm)	5/75/12/8
Outer core(Np/Pu/Cm)	7/92/1
Discharge burnup (MWd/kg)	
Inner core	64
Outer core	173
Actinide consumption (kg/yr)	
Pu-fissile	121
Pu-total	-55
Minor actinide	342
Burnup swing (% $\delta k$ )	1.04
Void worth (% $\delta k$ )	
BOEC	1.16
EOEC	1.51
Doppler ( $10^{-4} T \delta k / \delta T$ )	
BOEC	-3.19
EOEC	-3.15

Table XIII  
Fuel Composition of Decoupled Base Core

Isotope	Inner core		Outer core	
	Atom density ( $10^{24}\text{cm}^{-3}$ )	Fraction (%)	Atom density ( $10^{24}\text{cm}^{-3}$ )	Fraction (%)
$^{234}\text{U}$	2.3276E-04 <sup>a</sup>	3.08	9.2196E-06	0.36
$^{235}\text{U}$	4.5884E-05	0.61	1.6718E-06	0.07
$^{236}\text{U}$	3.6302E-05	0.48	1.3370E-06	0.05
$^{238}\text{U}$	3.1716E-08	0.00	1.2380E-09	0.00
$^{237}\text{Np}$	5.6839E-03	75.17	1.6948E-04	6.68
$^{236}\text{Pu}$	0.0000E+00	0.00	4.6719E-09	0.00
$^{238}\text{Pu}$	2.2506E-07	0.00	2.0889E-04	8.23
$^{239}\text{Pu}$	7.5849E-08	0.00	1.1958E-03	47.13
$^{240}\text{Pu}$	8.3310E-06	0.11	5.2813E-04	20.81
$^{241}\text{Pu}$	4.7635E-09	0.00	2.9405E-04	11.59
$^{242}\text{Pu}$	5.3103E-09	0.00	1.0258E-04	4.04
$^{241}\text{Am}$	4.7202E-04	6.24	7.6136E-06	0.30
$^{242\text{m}}\text{Am}$	2.4800E-06	0.03	1.6950E-08	0.00
$^{243}\text{Am}$	4.6590E-04	6.16	5.6975E-07	0.02
$^{242}\text{Cm}$	1.9419E-07	0.00	3.9783E-09	0.00
$^{243}\text{Cm}$	4.4281E-06	0.06	1.0886E-07	0.00
$^{244}\text{Cm}$	4.3143E-04	5.71	1.2013E-05	0.47
$^{245}\text{Cm}$	1.1793E-04	1.56	3.9201E-06	0.15
$^{246}\text{Cm}$	5.9245E-05	0.78	2.0951E-06	0.08

<sup>a</sup> read as  $2.3276 \times 10^{-4}$

Table XIV  
Effect of Moderating Pins in Outer Core

	BASE	M78	M180
Power (MWth)	900	900	900
Cycle length (days)	304	304	304
Number of batches	3	3	3
Number of drivers			
Inner core	114	114	114
Outer Core	114	114	114
BeO pins per outer core assembly	0	78	180
Actinide consumption (kg/yr)			
Pu-fissile	135	139	168
Pu-total	-41	-37	1
Minor actinide	342	323	283
Burnup swing (% $\delta k$ )	1.04	1.82	3.67
Void worth (% $\delta k$ )			
BOEC	1.16	1.00	0.47
EOEC	1.51	1.55	1.23
Doppler ( $10^{-3} T \delta k / \delta T$ )			
BOEC	-0.32	-0.70	-2.08
EOEC	-0.32	-0.63	-1.75

Table XV  
Effect of Outer Core Size

	BASE	O138	O210
Power (MWth)	900	900	900
Cycle length (days)	304	304	304
Number of batches	3	3	3
Number of drivers			
Inner core	114	114	114
Outer core	114	138	210
Number of control rods	42	66	66
Actinide consumption (kg/yr)			
Pu-fissile	135	140	147
Pu-total	-41	-26	-18
Minor actinide	342	314	306
Burnup swing (% $\delta k$ )	1.04	1.40	1.61
Void worth (% $\delta k$ )			
BOEC	1.16	0.72	1.18
EOEC	1.51	1.05	1.62
Doppler ( $10^{-3}T \delta k / \delta T$ )			
BOEC	-0.32	-0.34	-0.31
EOEC	-0.32	-0.33	-0.31



Table XVI  
General Specifications of Final MAB Model

Core concept	Decoupled annular
Reactor power (MWth)	1200
Fuel height (cm)	91.44
Number of assemblies	
Inner core	114
Outer core	138
Number of control rods	66
Control rod parking material	HT-9
Structural material	HT-9
Capacity factor (%)	80
Cycle length (days)	304
Fuel residence time (cycles)	3

Table XVII  
Fuel Assembly Data of Final MAB Model

	Inner core	Outer core
Fuel type	U/Np/Am/Cm +25%Zr	U/Np/Pu/Cm +25%Zr
Mass ratio (U/Np/Pu/Am/Cm)	5/71/0/15/9	1/8/90/0/1
Volume ratio (Fuel/coolant/structure)	38/36/26	13/72/15
Number of pins per assembly	271	162
Fuel pin diameter (cm)	0.724	0.544
Cladding thickness (cm)	0.056	0.043
Pitch/diameter ratio	1.18	1.96
Fuel smear density (% T.D.)	75	75
Assembly lattice pitch (cm)	15.4686	15.4686

Table XVIII  
Fuel Composition of Final MAB Model

Isotope	Inner core		Outer core	
	Atom density ( $10^{24} \text{cm}^{-3}$ )	Fraction (%)	Atom density ( $10^{24} \text{cm}^{-3}$ )	Fraction (%)
$^{234}\text{U}$	2.7395E-04 <sup>a</sup>	3.63	1.4224E-05	0.56
$^{235}\text{U}$	5.3394E-05	0.71	2.6069E-06	0.10
$^{236}\text{U}$	4.2162E-05	0.56	2.0733E-06	0.08
$^{238}\text{U}$	3.6006E-08	0.00	1.8415E-09	0.00
$^{237}\text{Np}$	5.3871E-03	71.40	2.0370E-04	8.02
$^{236}\text{Pu}$	0.0000E+00	0.00	3.9671E-09	0.00
$^{238}\text{Pu}$	1.7186E-07	0.00	2.3588E-04	9.28
$^{239}\text{Pu}$	8.2770E-08	0.00	1.1432E-03	44.98
$^{240}\text{Pu}$	8.8380E-06	0.12	5.2560E-04	20.68
$^{241}\text{Pu}$	4.9449E-09	0.00	2.7791E-04	10.94
$^{242}\text{Pu}$	5.6265E-09	0.00	1.0289E-04	4.05
$^{241}\text{Am}$	5.6880E-04	7.54	7.5428E-06	0.30
$^{242\text{m}}\text{Am}$	3.0582E-06	0.04	3.0581E-08	0.00
$^{243}\text{Am}$	5.6166E-04	7.44	8.7251E-07	0.03
$^{242}\text{Cm}$	1.4922E-07	0.00	2.3248E-09	0.00
$^{243}\text{Cm}$	4.6273E-06	0.06	1.4191E-07	0.01
$^{244}\text{Cm}$	4.5769E-04	6.07	1.6445E-05	0.65
$^{245}\text{Cm}$	1.2242E-04	1.62	5.3990E-06	0.21
$^{246}\text{Cm}$	6.0464E-05	0.80	2.8664E-06	0.11

<sup>a</sup> read as  $2.7395 \times 10^{-4}$

Table XIX

Equilibrium Cycle Performance Parameter of Final MAB Model

	Inner core	Outer core
Power fraction (%)		
BOEC	45.64	52.31
EOEC	54.18	43.77
Peak linear power (kW/m)		
BOEC	33.3	40.3
EOEC	33.9	34.0
Power peaking factor		
BOEC	1.72	1.31
EOEC	1.47	1.32
Peak flux ( $10^{15}/\text{cm}^2\text{sec}$ )		
BOEC	3.33	3.43
EOEC	3.33	3.36
Breeding ratio	0.03	0.12
Discharge burnup (MWD/kg)	82.08	198.70

Table XX

## Safety Performance Parameters of Final MAB Model

	BOEC	EOEC
Burnup swing (% $\delta k$ )		1.19
Void worth (% $\delta k$ )	0.74	1.17
Doppler ( $10^{-3}T \delta k / \delta T$ )	-0.35	-0.32

Table XXI  
Thermal Property Data

Fuel thermal conductivity (W/m <sup>o</sup> K)	22
Clad thermal conductivity (W/m <sup>o</sup> K)*	21
Coolant	
Inlet temperature (°K)	630
Bulk temperature (°K)	650
Density (kg/m <sup>3</sup> )	862
Thermal conductivity (W/m <sup>o</sup> K)	73
Specific heat (kJ/kg <sup>o</sup> C)	1.3
Velocity (m/sec)	6

\* at 750°K

Table XXII  
Effect of Outer Core Pin Size in Final MAB Model

Parameter	Fuel pins per assembly		
	91	127	162
Outer diameter (cm)	0.724	0.612	0.544
Clad thickness (cm)	0.056	0.048	0.043
Pin pitch (cm)	1.524	1.219	1.067
$P/D$	2.100	1.992	1.963
$A$ (cm <sup>2</sup> )	0.813	0.497	0.374
$Pw$ (cm)	1.138	0.963	0.853
$De$ (m)	0.029	0.021	0.018
$\dot{m}$ (kg/sec)	0.420	0.257	0.194
Pe	2,671	1,906	1,631
Nu	261	197	175
$h$ (W/m <sup>2</sup> K)	657,000	685,000	710,000
$\Delta T_{\text{coolant}}$ (°K)	58.7	86.9	81.8
$\Delta T_{\text{fuel}}$ (°K)	357	257	202
$T_{\text{fuel-center}}$ (°K)	1,046	974	913

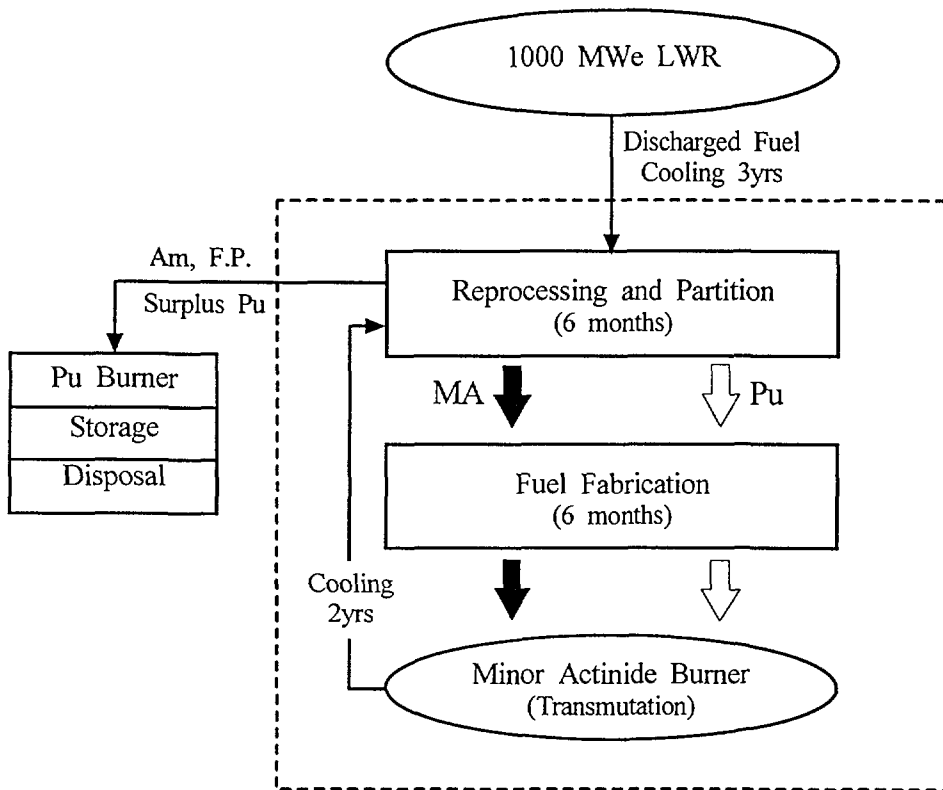
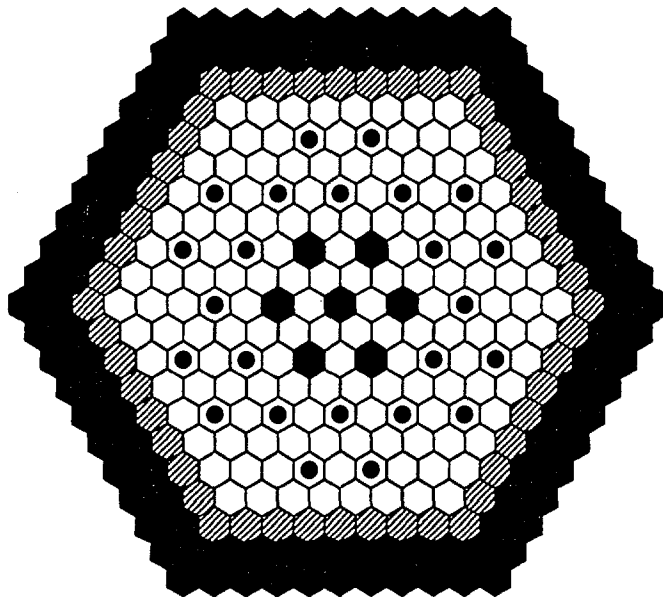


Fig.1 Mass Flow of MAB Fuel Cycle









- |                                                                                                 |                                                                                               |
|-------------------------------------------------------------------------------------------------|-----------------------------------------------------------------------------------------------|
|  Drivers     |  Reflector |
|  Control Rod |  B4C Block |

Fig.2 Horizontal View of Homogeneous Base Core

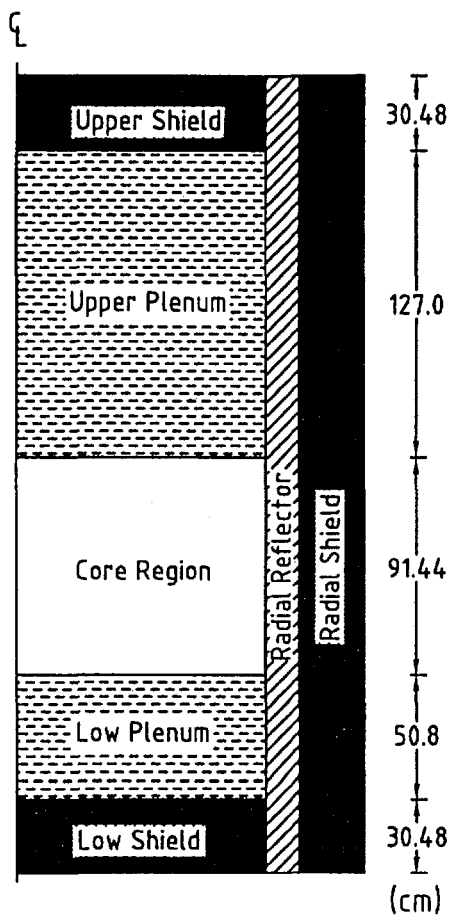
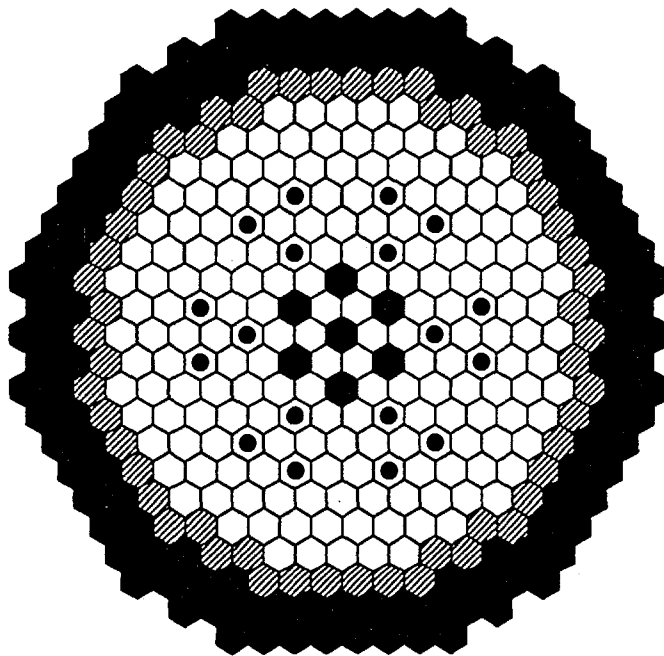


Fig.3 Vertical View of Homogeneous Base Core



- |   |             |   |           |
|---|-------------|---|-----------|
| ○ | Drivers     | ▨ | Reflector |
| ● | Control Rod | ■ | B4C Block |

Fig.4 Homogeneous Core Model with a Sodium Fraction of 0.469

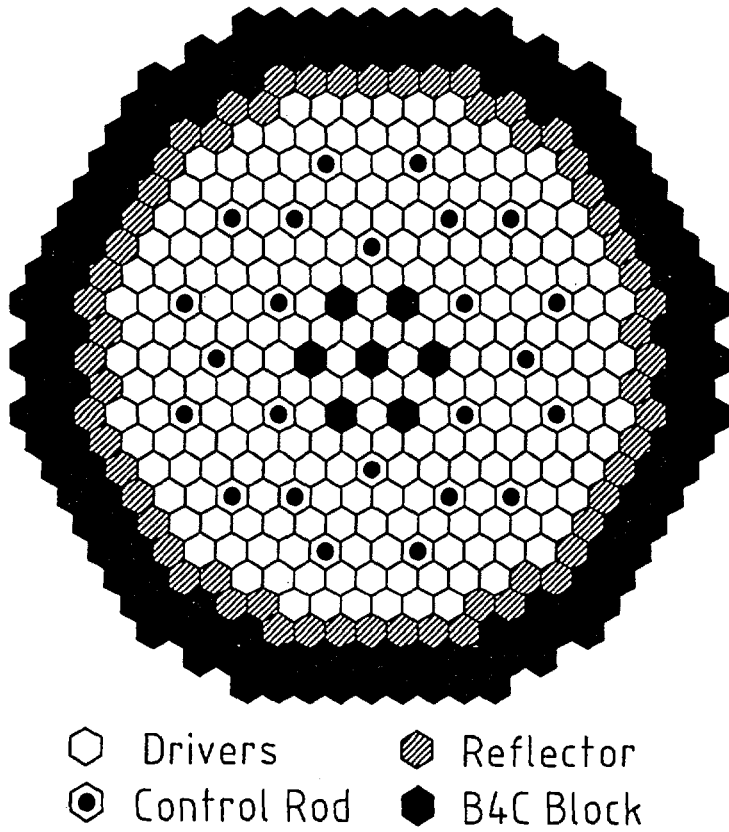


Fig.5 Homogeneous Core Model with a Sodium Fraction of 0.567

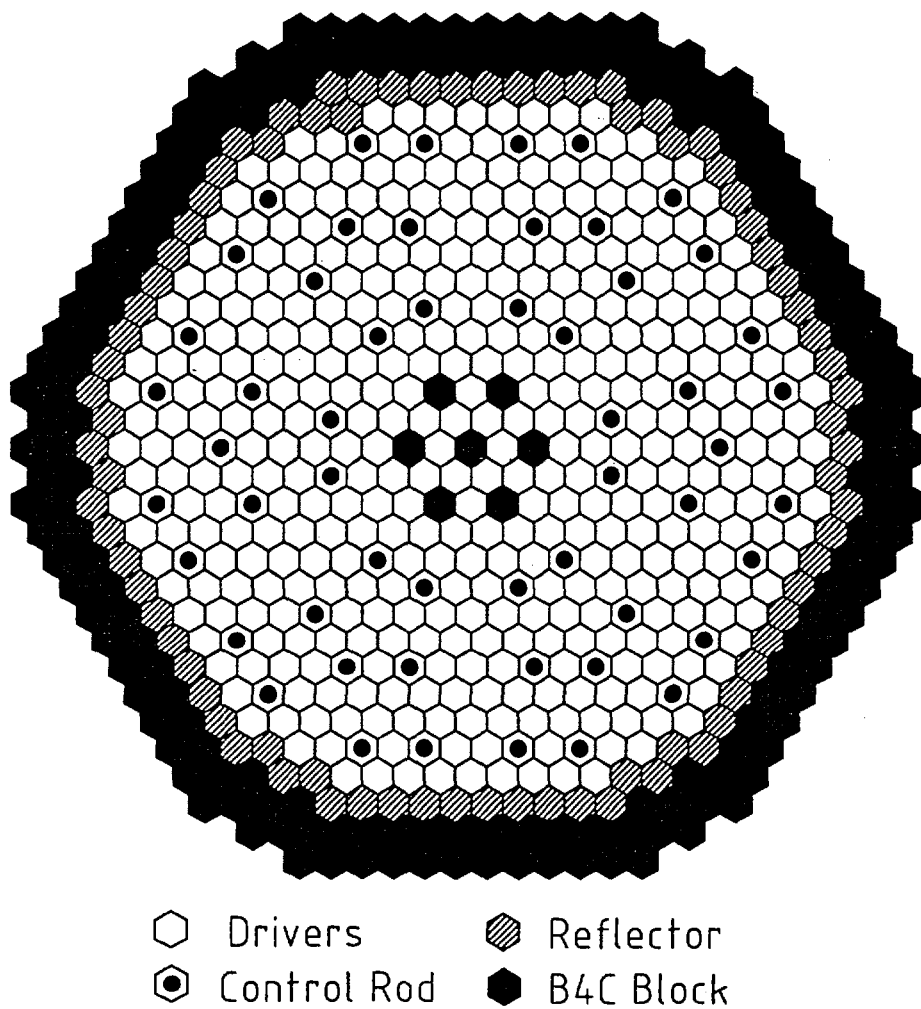


Fig.6 Homogeneous Core Model with a Sodium Fraction of 0.727

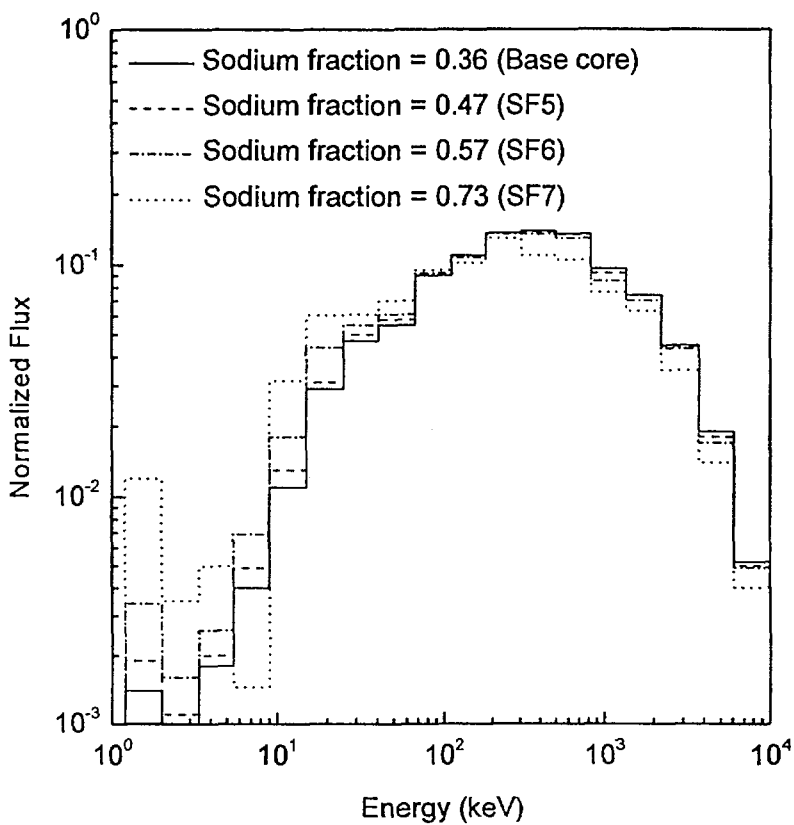


Fig.7 Spectrum Softening due to Sodium Fraction

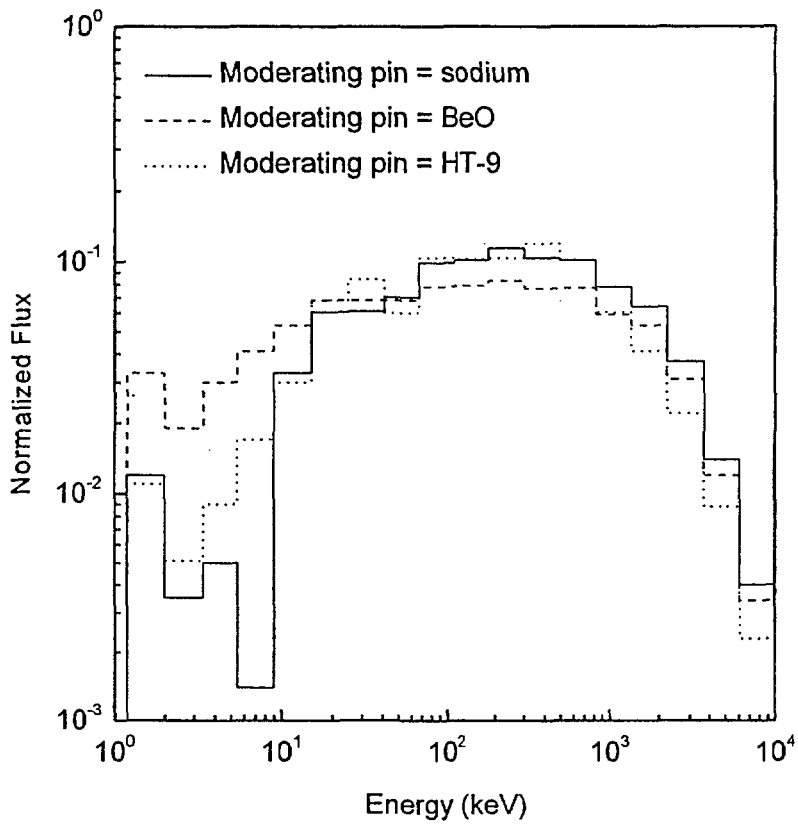
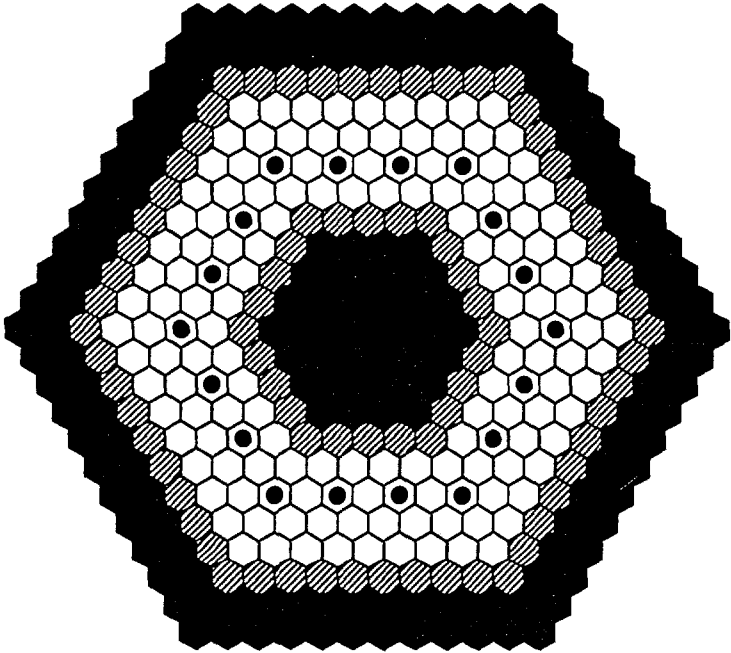


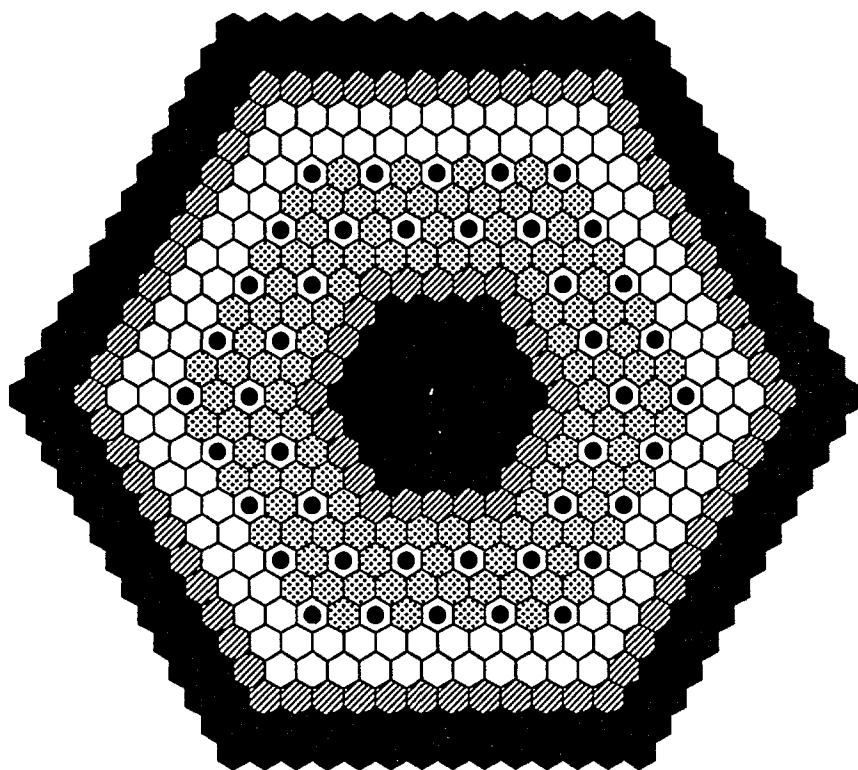
Fig.8 Spectrum Softening due to Moderating Pins



- Drivers
- ◐ Reflector
- Control Rod
- B4C Block

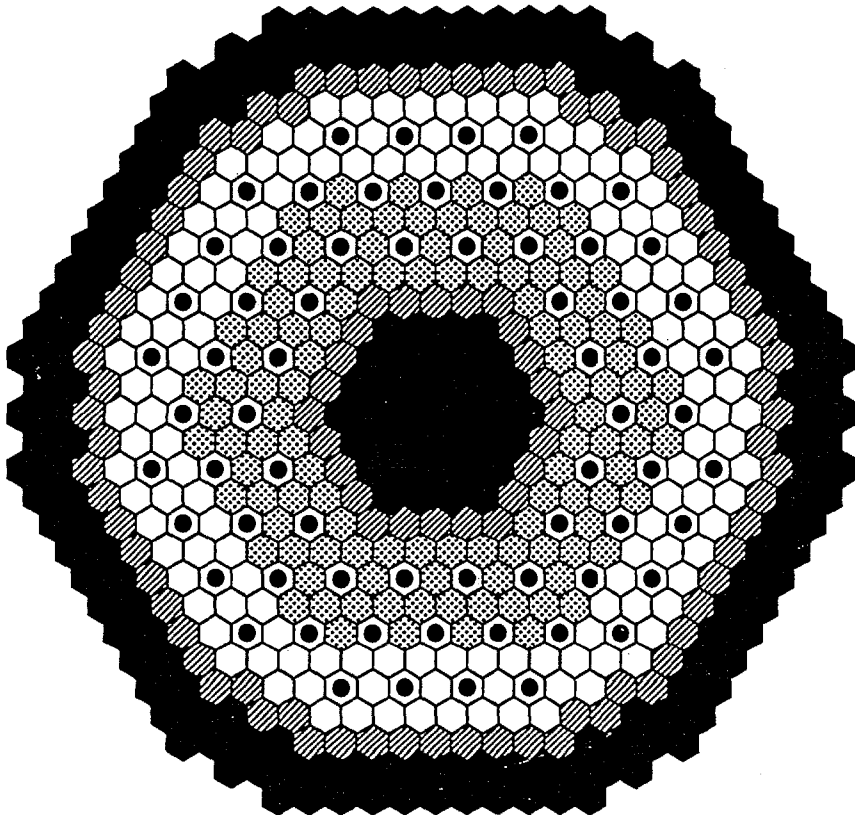
Fig.9 Annular Core Model





- |                                                                                     |             |                                                                                     |            |
|-------------------------------------------------------------------------------------|-------------|-------------------------------------------------------------------------------------|------------|
|  | Inner Core  |  | Outer Core |
|  | Control Rod |  | B4C Block  |
|  | Reflector   |                                                                                     |            |

Fig.10 Decoupled Base Core Model




-  Inner Core
-  Outer Core
-  Control Rod
-  Reflector
-  B4C Block

Fig.11 Horizontal View of Final MAB Model

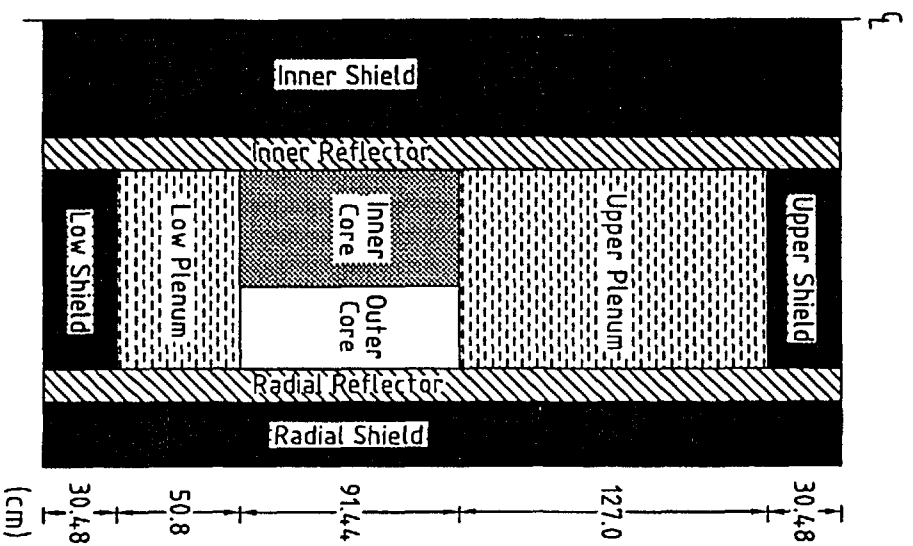


Fig.12 Vertical View of Final MAB Model

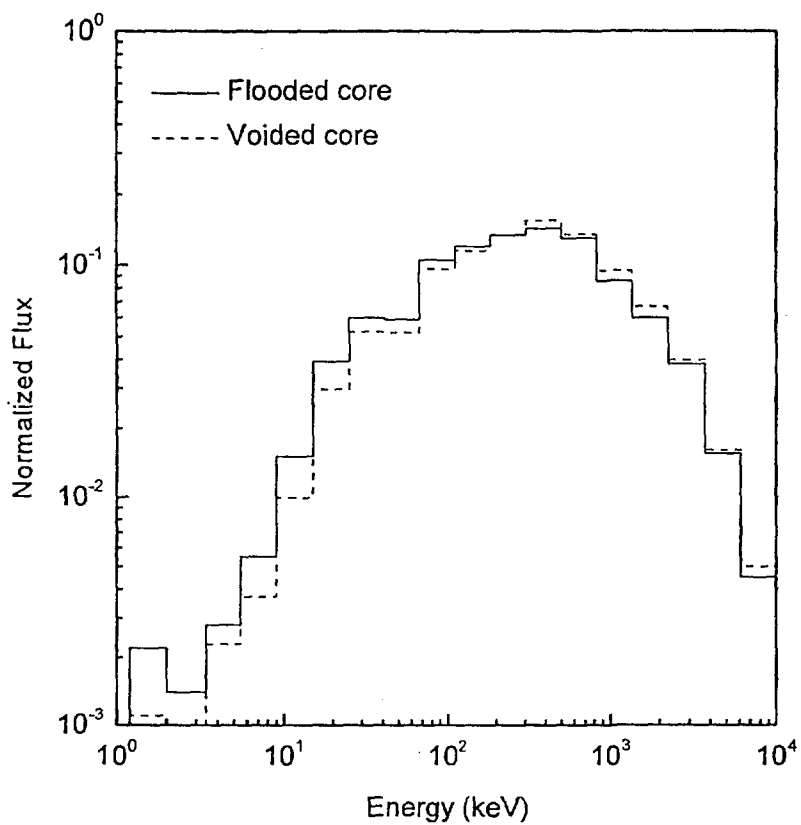


Fig.13 Spectrum Hardening in Inner Core

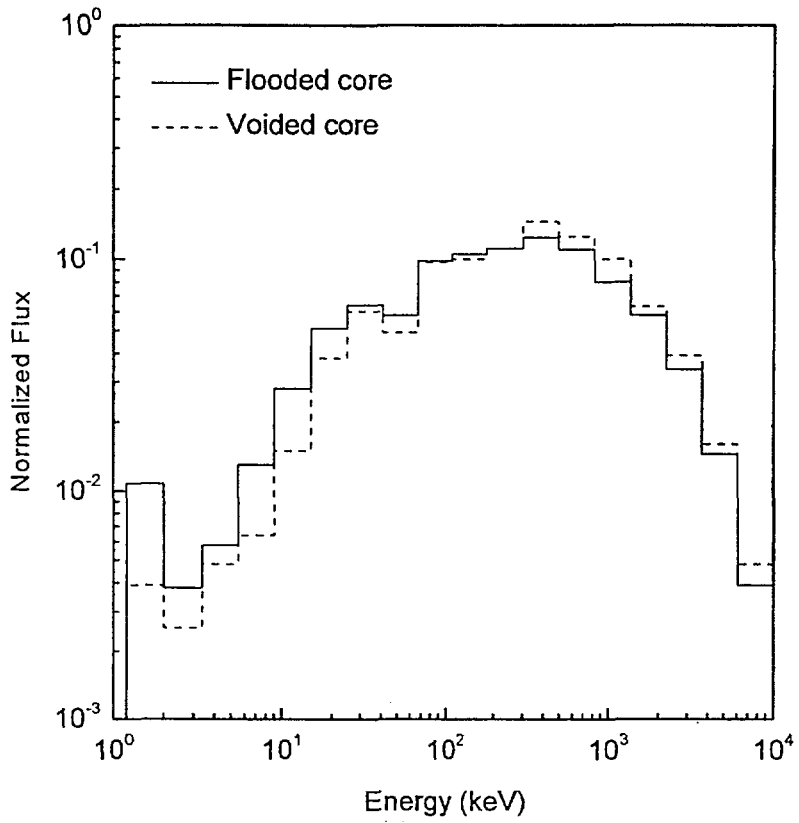


Fig.14 Spectrum Hardening in Outer Core

BIBLIOGRAPHIC INFORMATION SHEET											
Performing Org. Report No.		Sponsoring Org. Report No.		Standard Report No.		INIS Subject Code					
KAERI/TR-1111/98											
Title / Subtitle		Neutronics Design Study on a Minor Actinide Burner for Transmuting Spent Fuel									
Project Manager and Department		Hangbok Choi (DUPIC Fuel Compatibility Analysis)									
Researcher and Department											
Publication Place		Taejon		Publisher		KAERI		Publication Date		1998.8	
Page		76 p.		Ill. & Tab.		Yes( <input type="radio"/> ), No ( <input type="radio"/> )		Size		26 cm.	
Note											
Classified		Open ( <input type="radio"/> ), Restricted ( <input type="radio"/> ), Class Document				Report Type		Technical Report			
Sponsoring Org.						Contract No.					
Abstract (15-20 Lines)		<p>A liquid metal reactor was designed for the primary purpose of burning the minor actinide waste from commercial light water reactors. The design was constrained to maintain acceptable safety performance as measured by the burnup reactivity swing, the doppler coefficient, and the sodium void worth. Sensitivity studies were performed for homogeneous and decoupled core designs, and a minor actinide burner design was determined to maximize actinide consumption and satisfy safety constraints. One of the principal innovations was the use of two core regions, with a fissile plutonium outer core and an inner core consisting only of minor actinides. The physics studies performed here indicate that a 1200 MWth core is able to transmute the annual minor actinide inventory of about 16 LWRs and still exhibit reasonable safety characteristics.</p>									
Subject Keywords (About 10 words)		spent fuel, liquid metal reactor, minor actinide, neutronics design, void coefficient, doppler constant, transmutation									

서 지 정 보 양 식					
수행기관보고서번호	위탁기관보고서번호	표준보고서번호	INIS 주제코드		
KAERI/TR-1111/98					
제목 / 부제	사용후핵연료의 소멸처리를 위한 희소액티나이드소각로의 노물리설계에 관한 연구				
연구책임자 및 부서명	최항복 (DUPIC 핵연료 양립성 평가)				
연구자 및 부서명					
출판지	대전	발행기관	한국원자력연구소	발행년	1998.8
페이지	76 p.	도표	있음(○), 없음( )	크기	26 cm.
참고사항					
비밀여부	공개(○), 대외비( ), — 급비밀		보고서종류	기술보고서	
연구위탁기관			계약번호		
초록 (15-20줄내외)	<p>경수로사용후핵연료내에 존재하는 희소액티나이드를 연소하기위한 액체금속로에 대한 연구를 수행하였다. 원자로 설계는 주요 안전성 변수인 연소반응도증감, 도플러상수 그리고 보이드상수를 수용가능한 범위 이내로 유지하도록 수행하였다. 이를 위해 균질노심 및 분리노심 모델에 대한 민감도 계산을 수행하여 최종 노심을 확정하였다. 최종노심의 특징은 노심이 플루토늄을 주로 포함하는 외부노심과 희소액티나이드를 주로 포함하는 내부노심의 구성이다. 이러한 노심에 대한 노물리 해석 결과, 1200 MWth 액체금속로의 경우 매년 경수로 16기에서 방출되는 희소액티나이드를 연소시킬수 있으며 노심의 안전성 변수도 적절이 유지되는 것으로 나타났다.</p>				
주제명키워드 (10단어내외)	사용후핵연료, 액체금속로, 희소액티나이드, 핵설계, 보이드상수, 도플러상수, 소멸처리				